PHYSICS AND ENGINEERING DESIGN FOR WENDELSTEIN VII-X

C. Beidler, G. Grieger, F. Herrnegger, E. Harmeyer,
J. Kißlinger, W. Lotz, H. Maaßberg, P. Merkel,
J. Nührenberg, F. Rau, J. Sapper, F. Sardei,
R. Scardovelli, A. Schlüter, H. Wobig

IPP 2/300 July 1989

MAX-PLANCK-INSTITUT FÜR PLASMAPHYSIK

8046 GARCHING BEI MÜNCHEN

MAX-PLANCK-INSTITUT FÜR PLASMAPHYSIK
Garching bei München

PHYSICS AND ENGINEERING DESIGN FOR WENDELSTEIN VII-X

C. Beidler, G. Grieger, F. Herrnegger, E. Harmeyer,
J. Kißlinger, W. Lotz, H. Maaßberg, P. Merkel,
J. Nührenberg, F. Rau, J. Sapper, F. Sardei,
R. Scardovelli, A. Schlüter, H. Wobig

IPP 2/300 July 1989

Die nachstehende Arbeit wurde im Rahmen des Vertrages zwischen dem Max-Planck-Institut für Plasmaphysik und der Europäischen Atomgemeinschaft über die Zusammenarbeit auf dem Gebiet der Plasmaphysik durchgeführt.

Table of contents

Abstract

At IPP Garching, the future experiment *Wendelstein VII-X* is being developed. A Helias configuration (Helical Advanced Stellarator) has been chosen because of its confinement and stability properties [1]. The goals of *Wendelstein VII-X* are to continue the development of the modular stellarator, to demonstrate the reactor capability of this stellarator line, and to achieve quasi-steady-state operation in a temperature regime above 5 keV. This temperature regime can be reached in *Wendelstein VII-X* if neoclassical transport plus the anomalous transport found in *Wendelstein VII-A* prevails. A heating power of 20 MW will be applied to reach the reactor-relevant parameter regime.

The magnetic field in *Wendelstein VII-X* has 5 field periods; other basic data are: major radius $R_0 = 6.5$ m, magnetic induction $B_0 = 3$ T and stored magnetic energy $W \approx 0.88$ GJ. The average plasma radius is 0.65 m. Superconducting coils are favoured because of their steady-state field, but pulsed water-cooled copper coils are also being investigated. Unlike planar circular magnetic field coils which experience only a radially directed force, twisted coils are subject to a lateral force component as well. Studies of various superconducting coil systems for Helias configurations have shown that the magnitudes of these radial and lateral force components are comparable. Based on a support model the mechanical stresses are calculated; all components of the stress tensor are of equal importance. Other studies are concerned with the many complex engineering aspects presented by the construction of non-planar superconducting coils.

I. Introduction

Wendelstein VII-X is a continuation of the Advanced Stellarator line, which has been developed at IPP Garching and successfully inaugurated with the construction of *Wendelstein VII-AS* . *Wendelstein VII-X* will go a step further than *Wendelstein VII-AS* , aiming to reach reactor-relevant parameter regimes and to demonstrate the reactor capability of modular stellarators. For this purpose, *Wendelstein VII-X* has been chosen to be large enough to give access for powerful heating and to allow quasi-steady-state operation. The main goals of the *Wendelstein VII-X* experiment are:

- to achieve quasi-steady-state operation in a reactor-relevant parameter regime with temperatures above 5 keV and densities above 10^{20} m^{-3},
- to demonstrate stable plasma equilibrium with $\langle\beta\rangle = 5\%$,
- to confine a plasma over a sufficiently long period of time, allowing extrapolation to reactor parameters,
- to control the plasma density and impurity content,
- to operate the magnetic field in steady state with a field generated by modular superconducting coils.

Wendelstein VII-X does not aim at ignition; therefore D-T reactions will not occur and provisions for handling radioactive materials need not be made. The temperature goal of 5 keV has been chosen since in a reactor this temperature regime must be reached with auxiliary heating only, without the assistance of α-particle heating which becomes important at higher temperatures. The aim of $\langle\beta\rangle = 5\%$ results mainly from economic considerations; since fusion power output grows with $\langle\beta\rangle$, the limits of $\langle\beta\rangle$, set by plasma instabilities, must be pushed as high as possible and explored experimentally.

Confinement is also a critical issue facing stellarator reactors; even given the assumption of neoclassical losses a careful optimization of particle orbits and the magnetic configuration must be made in order to reach ignition. Therefore, particular attention will be given to this topic in *Wendelstein VII-X* .

Another important issue is steady-state operation, which is one of the principal advantages of stellarator reactors. In the *Wendelstein VII-X* experiment this means a pulse duration of 20-30 seconds, since in this time all transient phenomena presumably have saturated and a steady state has been reached. Such a state may be endangered by continuous impurity release from the wall and impurity accumulation in the plasma center; control of these effects and a careful examination of the underlying mechanisms is a major goal of *Wendelstein VII-X* .

The envisaged pulse duration of the plasma, the available space for coils and relevance for future application in reactors has led to the decision to produce the magnetic field by modular superconducting coils. With a magnetic field of 3 T on axis and 6 T at the coils, it is possible to employ the existing technology of NbTi. Normal-conducting modular coils have been built already and are successfully in use on *Wendelstein VII-AS* . Based on feasibility studies made by industry, it is believed that extending this technique to larger experiments and superconducting coils does not present insurmountable difficulties.

II. The Principles of Optimization

Since plasma confinement and stability depend mainly on the properties of the magnetic field (e.g. rotational transform, shear, magnetic well, and the structure of B on the magnetic surfaces) a careful optimization of the magnetic field and the modular coils is required to simultaneously achieve the following desirable properties:

I. High quality of the magnetic surfaces.
This implies a confinement region with good magnetic surfaces and an average aspect ratio $A \lesssim 10$. If low-order rational surfaces are avoided, field errors cause only small islands which are considered to be harmless. For this purpose, the shear must be small but finite. A typical value is $\delta\iota/\iota = 0.1$.

II. Good finite-β equilibrium properties.
A small Shafranov shift and a small variation of the rotational transform with $\langle\beta\rangle$ for vanishing net toroidal current will yield a high equilibrium-$\langle\beta\rangle$ limit. This is possible when $< j_{\|}^2/j_{\perp}^2 > \leq 1$, which is primarily achieved by a suitable combination of helical curvature and elliptical flux surface cross-section; see for example [1, 2].

III. Good MHD-stability properties.
MHD stability in low-shear stellarators is mainly provided by a magnetic well. A vacuum field magnetic well of approximately 2% can be created by exploiting the helical curvature and suitably chosen indentation and triangularity of the flux surfaces. Magnetic well stabilization of resistive interchange modes at high $\langle\beta\rangle$ values requires sufficiently reduced parallel current density. Side conditions on the magnetic surfaces (aspect ratio, local curvature, local flux surface spacing) have to be observed in order to avoid ideal ballooning instabilities becoming more restrictive than Mercier instabilities.

IV. Reduced neoclassical transport in the $1/\nu$ regime.
Isodynamic configurations [3] have $j_{\|} = 0$ and classical instead of neoclassical losses but apparently cannot be closely approximated at a finite aspect ratio because it is impossible to eliminate all poloidal variation from B in a curved system. The existence of quasi-helically-symmetric stellarators [4] implies that toroidal stellarators without $1/\nu$ transport exist. The general nonaxisymmetric stellarator can be characterized by a normalized ripple transport coefficient $D_R = 1.65\delta_e^{3/2} L^*$($L^*$= normalized mean free path) with the magnitude of the equivalent ripple δ_e determined by Monte Carlo simulation of electron transport in the long-mean-free-path (*lmfp*) regime. This ripple must be kept small, typically 2% or smaller at half of the minor radius, to guarantee sufficiently good neoclassical energy confinement. This can be achieved by reducing the radial drift velocity of particles.

V. Small bootstrap current in the *lmfp* regime.
The bootstrap current alters the rotational transform and for this reason it is particularly dangerous in low-shear stellarators. While axisymmetric configurations exhibit a bootstrap current which increases the rotational transform, quasi-helically-symmetric stellarators show a 'reversed' bootstrap current, i.e. one which decreases the rotational transform. It is possible to reduce the bootstrap current to a tolerable level by a proper combination of helical components and toroidal curvature effects in B on every magnetic surface.

VI. Good modular coil feasibility

Generally, strong geometrical shaping of the plasma boundary will improve confinement and stability properties while it adversely affects coil feasibility. Thus, side conditions on the shaping parameters on the plasma boundary have to be used to qualitatively ensure coil feasibility. Important issues for selecting the coil geometry are the minimum distance between the coils and the plasma and the minimum radius of curvature of the coils.

A further necessary prerequisite for an experimental device is a sufficiently broad range of accessible and variable magnetic field parameters, (e.g. field strength, rotational transform and axis position).

In designing *Wendelstein VII-X* , a simultaneous optimization of all properties mentioned above is possible, however some compromises must be accepted. For example, the necessity of small bootstrap current requires some deviation from quasi-helical symmetry and therefore an increase of neoclassical $1/\nu$ transport occurs. In *Wendelstein VII-X* , the resulting enhancement of the plasma losses is small, however confinement of highly-energetic trapped particles, e.g. α particles in a Helias reactor, may be strongly degraded by these asymmetries.

III. Basic Data of Wendelstein VII-X

The magnetic field configuration of *Wendelstein VII-X* differs from *Wendelstein VII-AS* mainly in the shape of the magnetic surfaces and in the existence of a helix-like magnetic axis. This Helias concept [1] (Helias = Helical Advanced Stellarator), extends the principle of minimum Pfirsch-Schlüter current to its maximum while it preserves MHD stability by maintaining a magnetic well. Helias configurations, which — as candidates for *Wendelstein VII-X* — have been investigated for 4, 5 and 6 field periods [5], are characterized by a small Shafranov shift and a small change of the rotational transform with finite $\langle\beta\rangle$. Configurations which are stable up to an average $\langle\beta\rangle$ of 9% (resistive interchange modes) have been found. In the special case of quasi-helically-symmetric configurations [4] neoclassical transport is very low and comparable to axisymmetric configurations since trapped particles are on confined orbits. Other Helias configurations are more of the 'linked-mirror' type [1,2,6] with poloidally closed mod-B contour lines. Furthermore, Helias configurations with very small bootstrap currents for all plasma radii have been found.

For all these reasons, a Helias configuration with 5 field periods has been selected for *Wendelstein VII-X* . The choice of 5 field periods is mainly dictated by resistive interchange and ideal ballooning modes, which lead to $\langle\beta\rangle$ limits below or equal to 3% for 4 field period configurations. Otherwise, the 4-period case would be preferable due to the less complex geometrical properties of the coil system.

For the sake of experimental flexibility, provision has to be made for variation of the rotational transform. The rotational transform of 5-period Helias configurations lies between 0.7 and 1.4 with a shear of $\delta\iota/\iota < 0.2$. A variable rotational transform can be achieved by either dividing the modular coils in an upper and lower winding pack and feeding each one separately with current or by adding a separate coil system which superimposes a toroidal field parallel or antiparallel to the field of the modular coils. The latter solution has been chosen for *Wendelstein VII-X* ; by superimposing a field of 10%, the rotational transform can be varied by $\pm 25\%$.

The number of modular coils per field period is driven in opposite directions by the desire for maximum distance between adjacent coils for heating and diagnostics purposes and the necessity to minimize the magnetic field ripple arising from these gaps. A compromise has been found with 12 coils per period.

A heating power of at least 20 MW is necessary to reach a reactor-relevant parameter regime in *Wendelstein VII-X* . For this reason, the geometric dimensions of the device have been chosen large enough to give access to heating schemes like neutral beam injection and to allow for heat removal systems. Furthermore, the distance between the plasma and the wall must be made as large as possible to keep wall loading and impurity influx low.

Collecting all physical arguments, a magnetic field on axis of 3 T and a major radius of 6.5 m (leading to an average plasma radius $a = 0.65$ m) have been chosen for *Wendelstein VII-X* . A representative coil system of *Wendelstein VII-X* and magnetic surfaces are shown in Figs. 1-2 for the case HS-5-8. In this specific version, the rotational transform on axis is $\iota = 1.02$ and $\iota = 1.18$ on the boundary. By a slightly different choice of the geometrical parameters another version, HS-5-7, with $\iota(0) = 0.75$ and $\iota(a) = 0.95$ is obtained. A list of important parameters for *Wendelstein VII-X* candidates is given in Table I.

Table I

			HS5-7	HS5-8
Average major radius	R_0	[m]	6.5	6.5
Average coil radius	r_c	[m]	1.30	1.30
Radial coil height	t	[m]	0.20	0.20
Lateral coil width	w	[m]	0.18	0.18
Average coil volume	V_c	[m^3]	0.33	0.33
Total coil volume	$n \cdot V_c$	[m^3]	19.7	19.8
Min. radius of curvature	ρ_c	[m]	0.27	0.28
Min. distance between coils	Δ_c	[m]	0.06	0.04
Coil number total / per FP	n/np		60/12	60/12
Total coil current	I_c	[MA]	1.73	1.73
Overall current density	j_c	[MA/m^2]	48.6	48.6
Total inductance (one-turn)	L	[μH]	591.	580.
Stored magnetic energy	W	[GJ]	0.88	0.87
Induction on axis	B_o	[T]	3.0	3.0
Max. induction at coil	B_m	[T]	5.7	5.8
Rotat. transform on axis	ι_o		0.75	1.02
Rotat. transform on boundary	ι_a		0.95	1.18
Average plasma radius	r_p	[m]	0.65	0.70
Average force density	$\langle f \rangle$	[MN/m^3]	76.	75.
Local max. force density	$\|f\|_m$	[MN/m^3]	274.	282.
Max. net force (one coil)	F_{res}	[MN]	3.8	4.0
Virial stress	σ_V	[MPa]	44.7	44.0

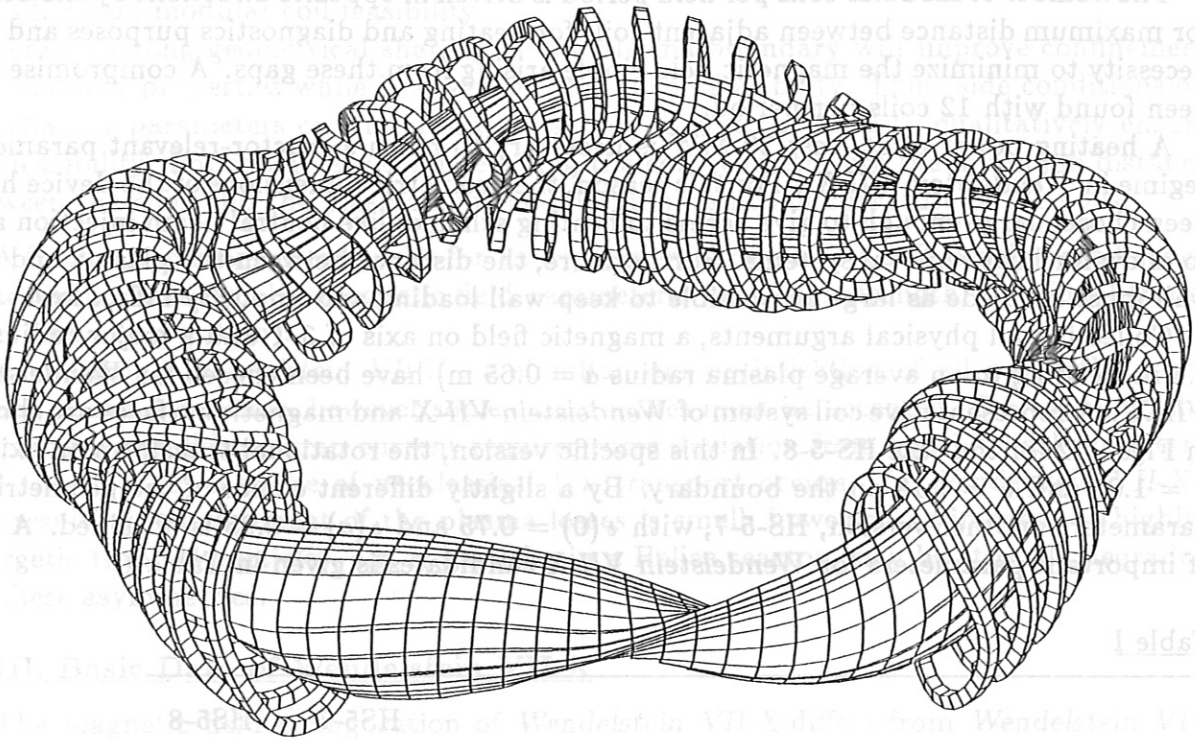

Fig. 1 *Coil system of HS-5-8 with 5 field periods, 12 coils per period. The geometrical data are listed in Table I.*

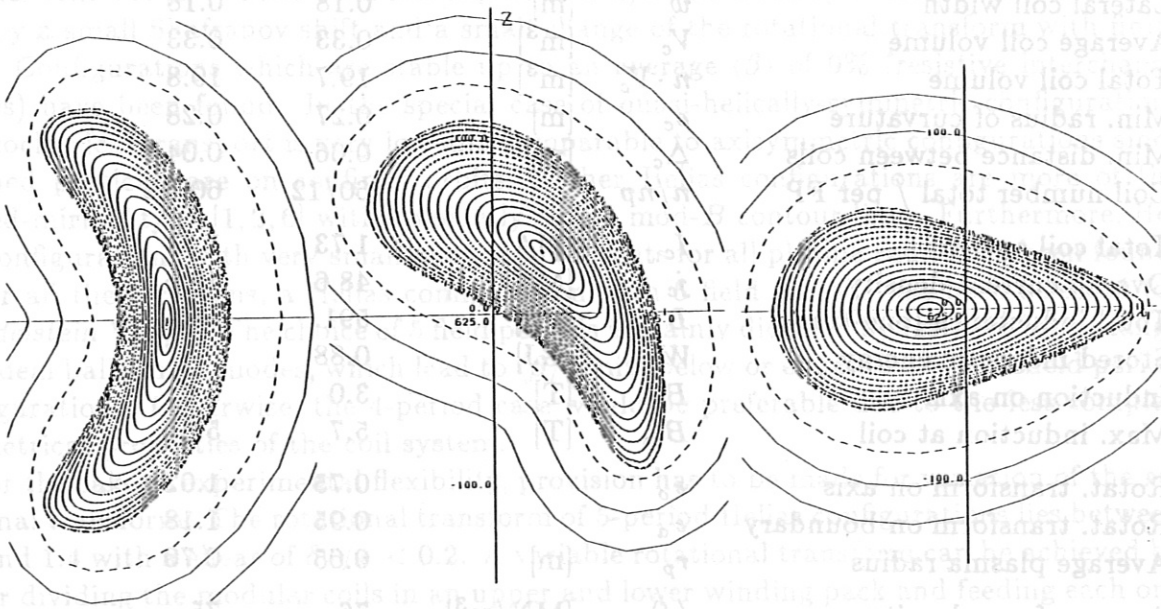

Fig. 2 *Cross section of the vacuum magnetic surfaces of HS-5-8 at: (left) the beginning of a field period, (center) 1/4 field period, (right) 1/2 field period. Solid lines: coil contours, dashed line: first wall.*

IV. MHD Equilibrium and Stability

Equilibrium in Helias configurations has been investigated using the VMEC-code which employs a fixed boundary [7]. Optimization of the shape of this boundary in a multidimensional parameter space with characteristically 10 variables led to the Helias stellarator [1]. Various examples of Helias equilibria are given in [8].

A common feature of Helias equilibria is the small Shafranov shift, Δ, which in conventional stellarators is given by the simple estimate $\Delta/a \approx \langle\beta\rangle A/2\iota^2$ (A =aspect ratio). Fig. 3 shows a 5-period Helias equilibrium with $\langle\beta\rangle = 0.15$.

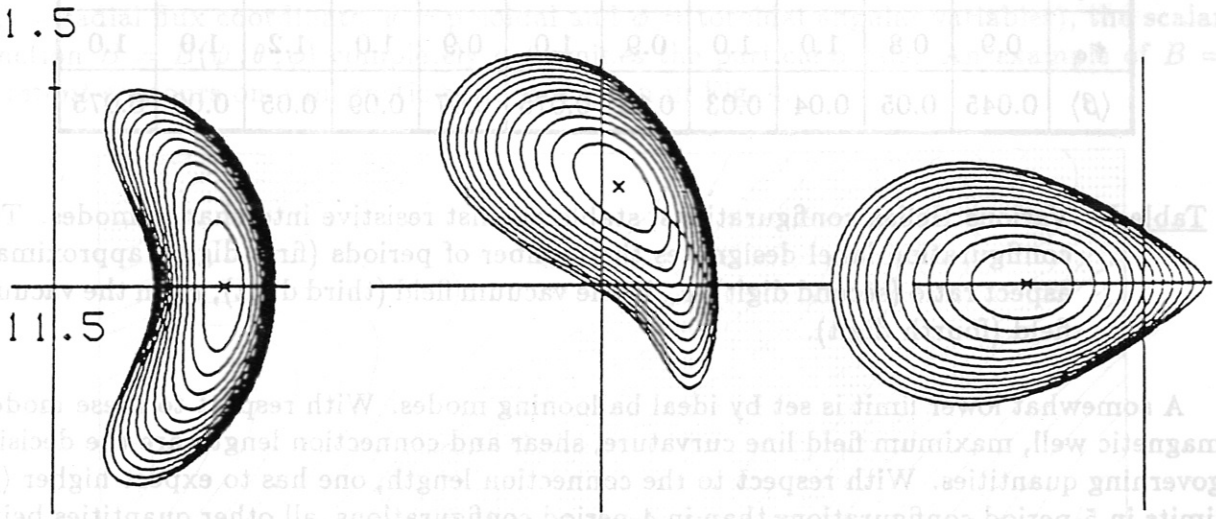

Fig. 3 *Example of a 5-field-period Helias equilibrium with $\beta = 0.15$ [7].*

A further characteristic of Helias equilibria is that the rotational transform is only slightly modified by the finite-$\langle\beta\rangle$ effect; this is particularly important in low-shear stellarators. Free-boundary equilibria of the Helias type have been studied [9] using the NEMEC Code. Due to the small Pfirsch-Schlüter current, the plasma pressure has little affect on the shape of the boundary. However, some questions still remain; these, in particular, concern the role of islands, stochasticity and a self-consistent description of these phenomena. In selecting the parameters of *Wendelstein VII-X* , the importance of islands in the plasma region can be kept small by avoiding low-order rational magnetic surfaces where large islands could otherwise occur. On the plasma boundary, however, islands may actually be helpful in controlling plasma density and impurities.

The MHD stability of Helias configurations has been investigated mainly on the basis of localized resistive interchange modes and ideal ballooning modes [7]; the analysis of global modes is under study. Since the shear in Helias configurations is rather small, MHD stability relies on the depth of the magnetic well and on the reduction of the Pfirsch-Schlüter current, both of which appear in the resistive interchange criterion (which approximately

coincides with Mercier's criterion). The magnetic well of a Helias vacuum field is rather small, typically less than 2%, so that $< j_{\parallel}^2/j_{\perp}^2 > \lesssim 1$, is necessary for stability against resistive interchange modes at sizeable β values. The resistive interchange stability limits of various Helias configurations with 4, 5 and 6 field periods are given in Table II.

	4889	4978	4881	4081	4099	5081	5099	5281	5912	6081	6281
M	4	4	4	4	4	5	5	5	5	6	6
$A \approx$	8	9.5	8	10	10	10	10	12	10	10	12
ι_o	0.8	0.7	0.8	0.8	0.8	0.8	0.8	0.8	1.1	0.8	0.8
ι_a	0.9	0.8	1.0	1.0	0.9	1.0	0.9	1.0	1.2	1.0	1.0
$\langle\beta\rangle$	0.045	0.05	0.04	0.03	0.05	0.075	0.07	0.09	0.05	0.06	0.075

Table II: Various Helias configurations, stable against resistive interchange modes. The configuration label designates the number of periods (first digit), approximate aspect ratio (second digit), ι_o in the vacuum field (third digit), ι_a in the vacuum field (fourth digit).

A somewhat lower limit is set by ideal ballooning modes. With respect to these modes, magnetic well, maximum field line curvature, shear and connection length are the decisive governing quantities. With respect to the connection length, one has to expect higher $\langle\beta\rangle$ limits in 5-period configurations than in 4-period configurations, all other quantities being kept fixed. In Table III, numerical results for the critical $\langle\beta\rangle$ values defined by MHD-ballooning modes are listed; in 4-period cases $\langle\beta\rangle = 3\%$ is the maximum stable value whereas in 5-period configurations $\langle\beta\rangle = 5\%$ can be achieved. This is the main reason for choosing 5 field periods in the design of *Wendelstein VII-X* .

	5281	HS4V12	4881	4081	5081	5099	6081	6281
$\frac{n}{m}$	$\frac{7}{8}$	$\frac{5}{6}$	$\frac{7}{8}$	$\frac{7}{8}$	$\frac{7}{8}$	$\frac{7}{8}$	$\frac{7}{8}$	$\frac{7}{8}$
$\langle\beta\rangle$	0.05	0.03	0.023	0.02	0.047	0.047	0.03	0.047

Table III: Ballooning mode numbers n, m and $\langle\beta\rangle$ values for marginal stability of the ballooning mode investigated.

Below the ideal ballooning mode $\langle\beta\rangle$ limit, the plasma will be unstable against resistive ballooning modes. However, the growth of these modes occurs on the resistive time scale rather than on the Alfvén time scale and it is generally believed that this instability leads to an increase of plasma losses instead of a violent destruction of the plasma column. Numerical studies of resistive ballooning modes in Helias configurations are in preparation [10]. Stability in Helias configurations is further endangered by drift modes excited by trapped particles.

V. Neoclassical Transport

Particle orbits in a magnetic field are the basis of neoclassical transport and therefore extensive studies of particle orbits have been carried out. In magnetic coordinates, ψ, θ, ϕ (ψ = radial flux coordinate, θ = poloidal and ϕ = toroidal angular variables), the scalar function $B = B(\psi, \theta, \phi)$ completely determines the particle orbits. An example of $B =$ *constant* contours on a magnetic surface is given in Fig. 4.

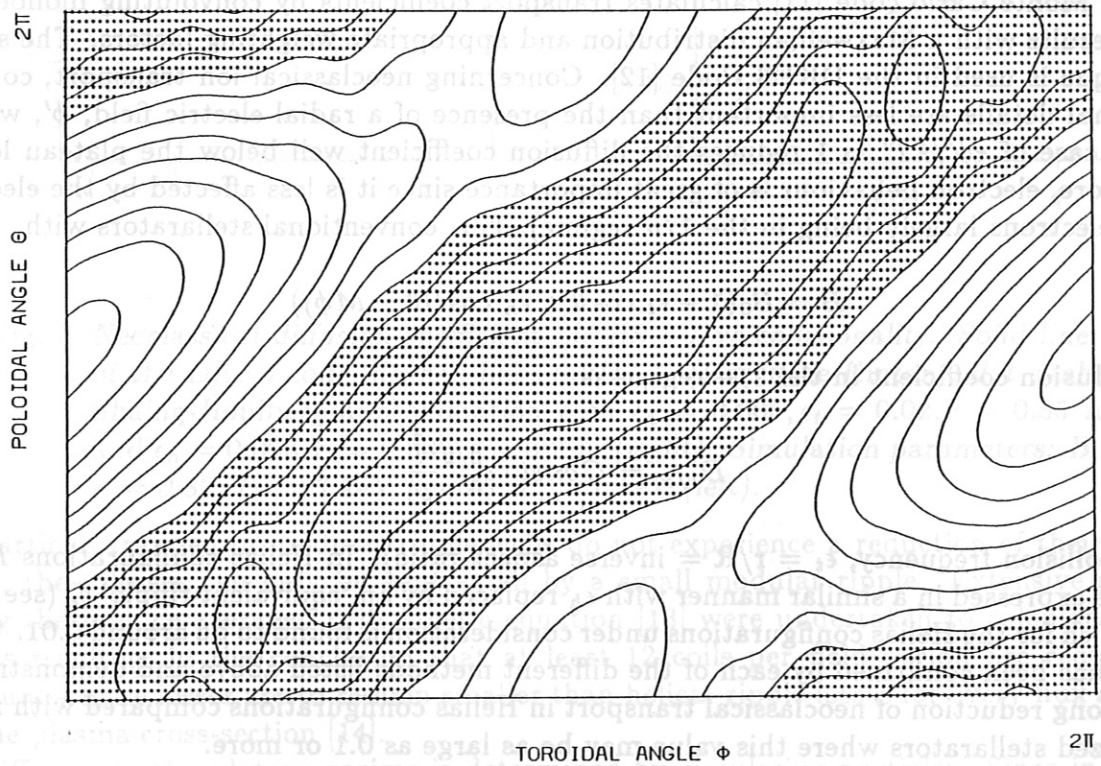

Fig. 4 *Contour lines of $B(\theta, \phi)$ = constant on a magnetic surface are shown over one field period of the configuration HS-5-8. Horizontal axis = toroidal angle, vertical axis = poloidal angle.*

Isodynamic configurations are characterised by $B(\psi, \phi)$, while in quasi-helically-symmetric cases, $B = B(\psi, \theta - M\phi)$. Trapped-particle orbits are of particular interest since transport in the *lmfp* regime is determined by these particles. All banana orbits would be confined if $B=B(\psi, \theta - M\phi)$ were to hold. However, small symmetry-breaking terms, $B_1(\psi, \theta, \phi)$, lead to neoclassical diffusion following the $1/\nu$ scaling. Concerning α - particles in a stellarator reactor, a situation similar to ripple-induced stochastic orbit losses in tokamaks may arise. In general, the function $B(\psi, \theta, \phi)$ varies if the plasma pressure increases and particle orbits may change. However, this is not typical of Helias configurations, where it is found that the Fourier spectrum of B experiences only small variations with finite $\langle\beta\rangle$. Particle orbits, and consequently neoclassical transport, depend only slightly on finite plasma pressure.

Neoclassical transport in Helias configurations has been studied by various methods:

- Monte-Carlo technique
- Analytical solution of the bounce-averaged drift kinetic equation
- Numerical solution of the drift-kinetic equation (DKES-code)

The Monte Carlo code [11] calculates transport coefficients by convoluting monoenergetic results with a Maxwellian distribution and appropriate weighting factors. The same technique is used in the DKES Code [12]. Concerning neoclassical ion transport, configurational details are less important than the presence of a radial electric field, ϕ', which in the case of $e\phi'/kT' \approx 1$ reduces the diffusion coefficient well below the plateau level. Therefore, electron behaviour is of great importance since it is less affected by the electric field (electrons largely being in the $1/\nu$ regime). For conventional stellarators with

$$B = B_0(1 - \epsilon_t \cos\theta + \epsilon_h \cos(l\theta - M\phi))$$

the diffusion coefficient in the $1/\nu$ regime is

$$D_{1/\nu} = Const \cdot \epsilon_h^{3/2} \frac{\epsilon_t^2}{\nu}$$

(ν = collision frequency, ϵ_t = r/R = inverse aspect ratio). In Helias configurations $D_{1/\nu}$ may be expressed in a similar manner with ϵ_h replaced by an 'equivalent ripple' δ_e (see Sec. II), which for the Helias configurations under consideration is found to be around 0.01. This result has been confirmed by each of the different methods listed above and demonstrates the strong reduction of neoclassical transport in Helias configurations compared with non-optimized stellarators where this value may be as large as 0.1 or more.

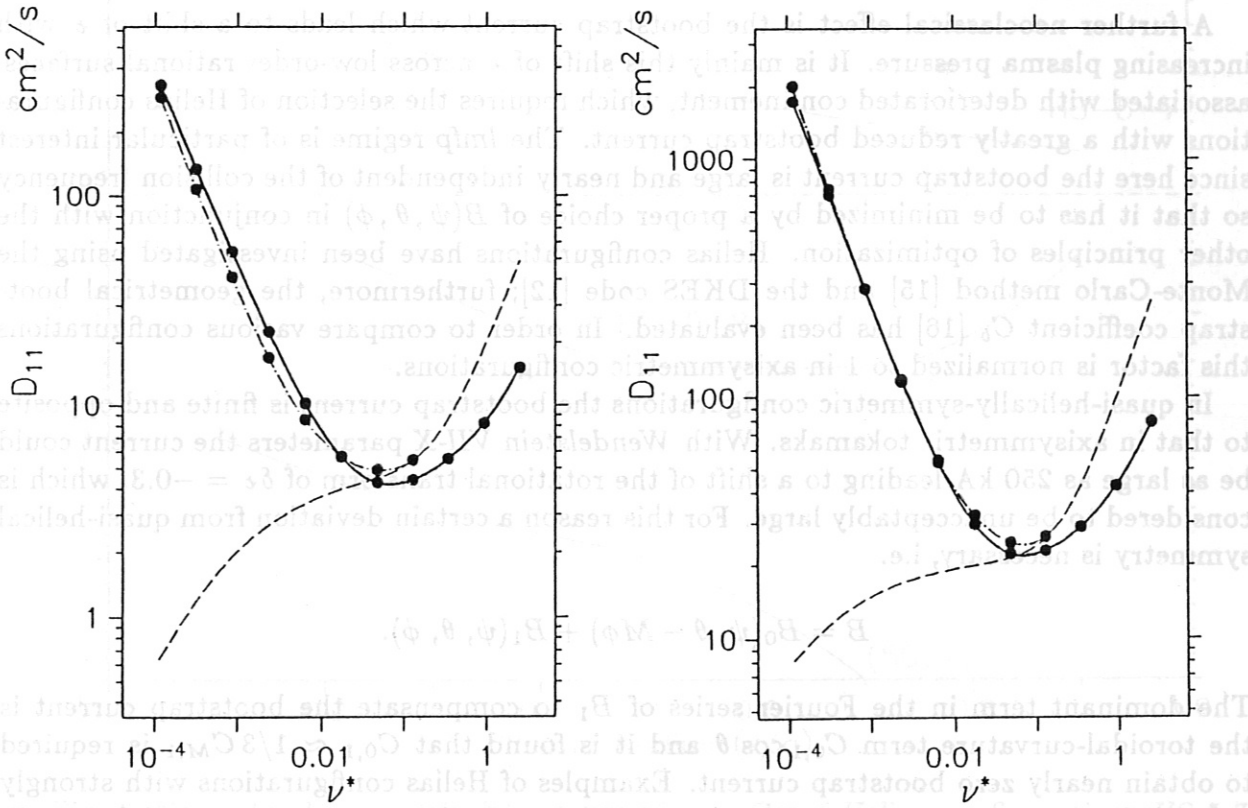

Fig. 5 *Neoclassical diffusion coefficient for HS-5-7 vs collisionality. Solid line: result of the DKES code, dashed line: $0.2D_{H,H}$ (Hazeltine-Hinton), dot-dashed line: Shaing-Houlberg approximation with $\epsilon_h = 0.005, \epsilon_t = 0.02, \bar{r} = 0.55$ m (left) and $\epsilon_h = 0.006, \epsilon_t = 0.006, \bar{r} = 0.2$ m (right). Simulation parameters: $B = 3$ T, $\iota = 0.82$, $T_e = 3$ keV (right), $T_e = 1$ keV (left).*

Particles trapped in modular ripple wells do not experience a reduction of their radial drift; these losses can only be kept small by a small modular ripple. Extensive studies using the bounce-averaged drift-kinetic equation [13] were undertaken to calculate these losses resulting in the conclusion that at least 12 coils per field period are required if modular-ripple losses are to remain smaller than helical-ripple losses for every flux surface in the plasma cross-section [14].

Diffusion in the plateau regime is determined by circulating particles. Since in Helias configurations the toroidal harmonic of B is much smaller than the inverse aspect ratio, these particles circulate on drift surfaces very close to magnetic surfaces and therefore a smaller radial diffusion is found than in standard stellarators. Reduction of plateau diffusion by a factor of 5 can be achieved; see Fig. 5. In summary, it can be stated that the *Wendelstein VII-X* experiment is being designed in such a way that its performance will not be seriously limited by neoclassical transport.

VI. The Bootstrap Current

A further neoclassical effect is the bootstrap current which leads to a shift of ι with increasing plasma pressure. It is mainly this shift of ι across low-order rational surfaces, associated with deteriorated confinement, which requires the selection of Helias configurations with a greatly reduced bootstrap current. The *lmfp* regime is of particular interest since here the bootstrap current is large and nearly independent of the collision frequency so that it has to be minimized by a proper choice of $B(\psi, \theta, \phi)$ in conjunction with the other principles of optimization. Helias configurations have been investigated using the Monte-Carlo method [15] and the DKES code [12]; furthermore, the geometrical bootstrap coefficient C_b [16] has been evaluated. In order to compare various configurations this factor is normalized to 1 in axisymmetric configurations.

In quasi-helically-symmetric configurations the bootstrap current is finite and opposite to that in axisymmetric tokamaks. With *Wendelstein VII-X* parameters the current could be as large as 250 kA leading to a shift of the rotational transform of $\delta\iota = -0.3$, which is considered to be unacceptably large. For this reason a certain deviation from quasi-helical symmetry is necessary, i.e.

$$B = B_0(\psi, \theta - M\phi) + B_1(\psi, \theta, \phi).$$

The dominant term in the Fourier series of B_1 to compensate the bootstrap current is the toroidal-curvature term $C_{0,1} \cos\theta$ and it is found that $C_{0,1} \approx 1/3\, C_{M,1}$ is required to obtain nearly zero bootstrap current. Examples of Helias configurations with strongly reduced bootstrap currents are HS-5-7 and HS-5-8. In Fig. 6 the geometrical factor C_b is shown; in both cases $|C_b| = 0.05$ is found, which means that the expected bootstrap current is 1/20 of the current in an equivalent axisymmetric configuration. Taking into account the achievable plasma parameters in *Wendelstein VII-X* , this would lead to a maximum bootstrap current of 50 kA.

Because of the assumptions and approximations of the theory, a further optimization of the bootstrap current by field shaping is irrelevant. A small residual bootstrap current can also be controlled experimentally by ECRH-current drive, a technique which has been successfully demonstrated on the *Wendelstein VII-AS* experiment [17].

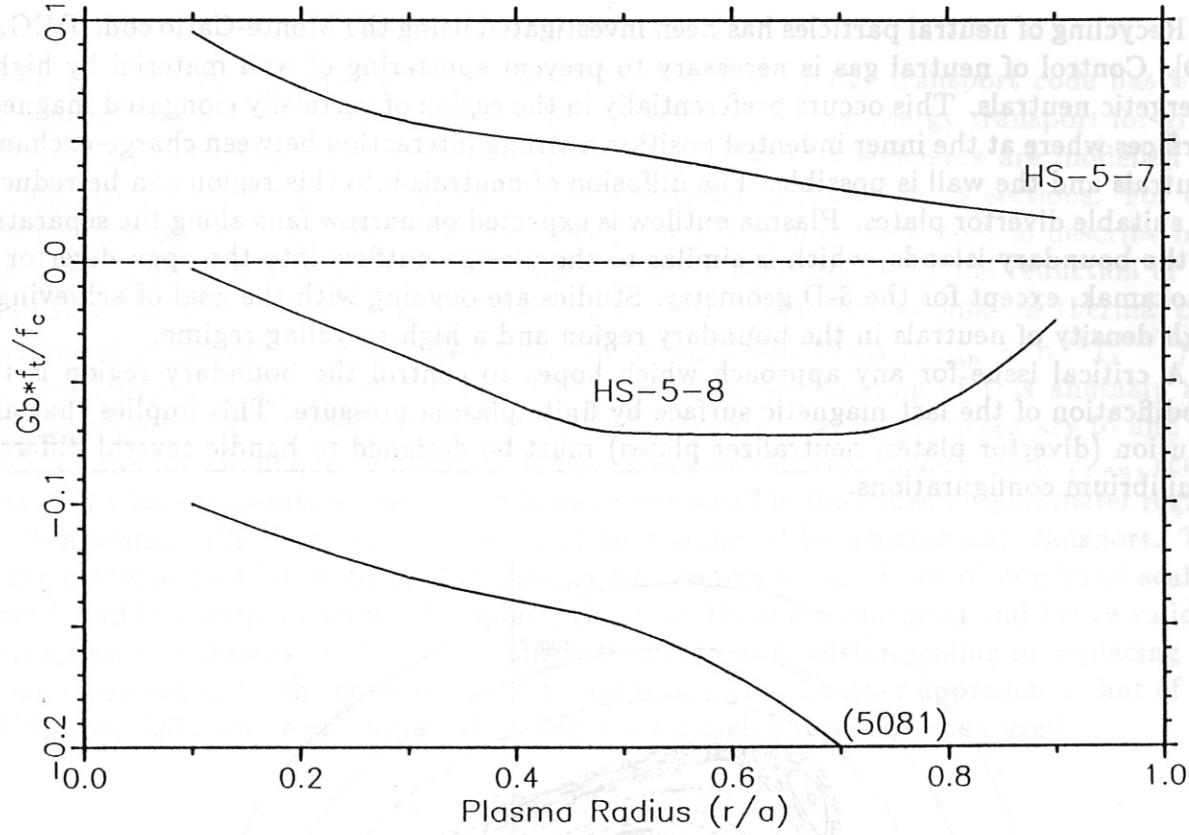

Fig. 6 *Normalized geometrical bootstrap factor C_b of Helias configurations HS-5-7, HS-5-8 and HS 5081. $C_b = 1$ in an axisymmetric tokamak with the same aspect ratio and rotational transform.*

VII. Boundary Region

A generic feature of Helias configurations is the existence of a last magnetic surface surrounded by a region of stochastic field lines, between which small islands or remnants of islands may exist, and a region of open field lines. Usually the stochastic region is very small and field lines started outside this stochastic region intersect the vacuum chamber after a few toroidal transits. The distance between the last magnetic surface and the first material wall depends critically on the value of the rotational transform on this last surface; a minimum distance of 10 cm is required to yield sufficient decoupling of plasma and wall. Fig.7 shows the standard case of HS-5-7, where at the boundary 5 islands with $\iota = 1.0$ exist and the last magnetic surface has more than 10 cm distance to the wall (dashed line). Field lines started in the ergodic region need several toroidal transits before they reach the wall and therefore a scrape-off layer of cold plasma surrounding the last magnetic surface will exist. The width of this scrape-off layer is determined by radial diffusion competing with parallel plasma flow to the wall or neutralizer plates. This situation resembles the scrape-off layer in tokamaks with an open divertor except for its three-dimensional geometry. Studies have been carried out to investigate the structure of the magnetic field in this boundary region and to identify the region of maximum wall loading by the outflowing plasma [18].

Recycling of neutral particles has been investigated using the Monte-Carlo code DEGAS [19]. Control of neutral gas is necessary to prevent sputtering of wall material by highly energetic neutrals. This occurs preferentially in the region of vertically elongated magnetic surfaces where at the inner indented position a strong interaction between charge-exchange neutrals and the wall is possible. The diffusion of neutrals into this region can be reduced by suitable divertor plates. Plasma outflow is expected on narrow fans along the separatrix of the boundary islands, which is similar to the plasma outflow into the open divertor of a tokamak, except for the 3-D geometry. Studies are ongoing with the goal of achieving a high density of neutrals in the boundary region and a high-recycling regime.

A critical issue for any approach which hopes to control the boundary region is the modification of the last magnetic surface by finite plasma pressure. This implies that any solution (divertor plates, neutralizer plates) must be designed to handle several different equilibrium configurations.

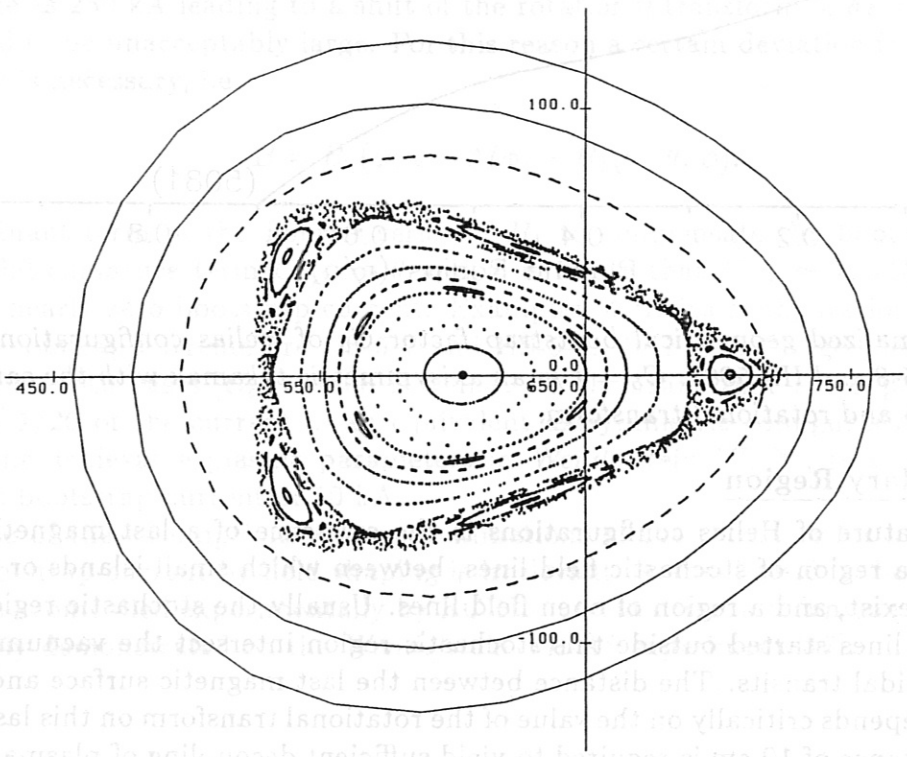

Fig. 7 *Cross section of magnetic surfaces of HS-5-7. Islands at the boundary correspond to* $\iota = 1.0$.

VIII. Prediction of Plasma Parameters

To predict plasma parameters in *Wendelstein VII-X* , a 1-D transport code has been developed which solves the combined equations of particle and energy transport for given radial source terms of particles and energy. The transport coefficients are modelled according to the results of neoclassical theory described in the previous sections. For this purpose the analytic approximations of Shaing and Houlberg were used to describe *lmfp* transport with ϵ_h being replaced by δ_e; at higher collision frequency the reduction of the plateau transport coefficients is also accounted for. Furthermore, anomalous thermal conduction of electrons — as has been found in *Wendelstein VII-A* ($\chi_{e,an} \sim n^{-1}T_e^{-2/3}$) — has been taken into account. There is no theoretical explanation of this anomaly and further experiments in *Wendelstein VII-AS* and other stellarators are necessary to find the scaling laws for anomalous transport. If the anomalous thermal conduction, $\chi_{e,an}$, scales inversely with temperature, its effect will be rather small in the expected parameter regime of *Wendelstein VII-X* and confinement will be dominated by neoclassical transport. The other extreme position is to predict plasma parameters on the basis of empirical scaling laws found in tokamaks under the assumption that these are universal and hence valid in currentless stellarators. This can be done with the Kaye-Goldston scaling by replacing the plasma current I_p by the equivalent rotational transform. Another approach is that of the LHS-group [20], where an empirical scaling law for stellarators has been used

$$\tau_E = 0.21 P^{-0.53} \bar{n}^{0.66} B^{0.53} a^2 R$$

(MW, T, $10^{20} m^{-3}$, m, s). Both scaling laws, Kaye-Goldston scaling and LHS-scaling, yield similar results.

On the basis of these transport models, the following results are obtained: With B = 2.5 T, $\bar{n} = 10^{20} m^{-3}$ and a heating power of P = 10 - 20 MW, the achievable average temperature is: 4 - 6 keV (neoclassical transport) and 1 - 2 keV (LHS-scaling). The energy confinement times are: $\tau_E = 0.5 - 1.0\, s$ (neoclassical transport) and $\tau_E = 0.1 - 0.3\, s$ (LHS-scaling). $\langle\beta\rangle$ values of 5% can be reached if the confinement time is 1 second for B = 2.5 T. At lower magnetic field this $\langle\beta\rangle$ value is obtained for shorter confinement times. With anomalous transport following the LHS-scaling the achievable $\langle\beta\rangle$ stays below 2% .

In summary, on the basis of neoclassical transport plus anomalous transport as found in Wendelstein VII-A, the plasma parameters listed in the goals of *Wendelstein VII-X* can be reached at a heating power of 10 - 20 MW. Anomalous transport following the Kaye-Goldston L-mode scaling or LHS-scaling would lead to much smaller values of achievable temperature.

IX. Plasma Heating

A heating power of 20 MW in *Wendelstein VII-X* will be provided by various methods: ECRH, NBI-heating and ICRH. To which extent each method will contribute is not yet decided. This decision will be made based on results obtained with current stellarator experiments.

ECRH is necessary to provide a target plasma for neutral beam injection; for this purpose only a small power (1 MW) is needed. Neutral beam injection in *Wendelstein VII-X* has been designed starting from the experience with ASDEX-Upgrade sources [21] (6 MW-units, 55 keV full energy, 10 seconds pulse length). Since special coils of the type employed on *Wendelstein VII-AS* are not foreseen for *Wendelstein VII-X* , the injection angle is nearly perpendicular to the magnetic field. The available space between coils allows an injection angle of 20 degrees, which is sufficient to ensure that most of the high energy particles will be born on circulating orbits. The aim of injection heating is to achieve a high-$\langle\beta\rangle$ plasma and to explore plasma stability at the stability limit. In this context, the density rise which is necessarily correlated with neutral beam injection (for the planned heating power a particle influx of $\sim 10^{21}$ per second is expected) is tolerable or even useful since high-$\langle\beta\rangle$ values can best be achieved at high density and low temperature.

Furthermore, testing $\langle\beta\rangle$ limits or stability limits does not require steady-state operation; therefore the density rise and the associated power loss by impurity radiation is not considered as a serious obstacle to this particular goal of *Wendelstein VII-X* .

ECRH is an appropriate heating scenario in *Wendelstein VII-X* for quasi-steady-state operation at high temperature with the plasma in the *lmfp* regime. Calculations show that this can be reached at a heating power of 10 MW. Further parameters of ECRH are: second harmonic heating at f = 140 GHz, B = 2.5 T and a maximum plasma density n(0) = $10^{20} m^{-3}$. Gyrotrons at this frequency are being developed for *Wendelstein VII-AS* ; further development towards power units of at least 1 MW each is necessary for application to *Wendelstein VII-X* . A further application of ECRH is current drive, which has been investigated for *Wendelstein VII-X* parameters [22]. These results indicate that at $\langle\beta\rangle$ = 5%, a current drive efficiency of 10 kA per MW heating power should be achievable, which is sufficient to control the residual bootstrap current.

As a third heating scenario, ICRH has been investigated [23]. The frequency regime is 38 to 76 MHz with units of 2 MW power. This allows second harmonic heating of hydrogen and deuterium and also minority heating of H in D at a magnetic field of 2.5 T.

Geometrical access to *Wendelstein VII-X* is provided for all heating schemes, since with 12 coils per field period the largest portholes are 40 x 80 cm^2. Therefore, application of all three heating schemes is planned in *Wendelstein VII-X* , either each one separately or in combination. To a large extent the planning will make use of the hardware and the expertise developed at IPP Garching in order to avoid expensive R and D programs for new heating sources.

X. The Modular Coils of Wendelstein VII-X

10.1 Methods for Finding Coils

The traditional approach to constructing stellarator fields starts from coils. Prescribing the geometry of current filaments by a so-called 'winding law', the magnetic field is calculated by using Bio-Savart's formula. A typical stellarator magnetic field with twist of the field lines — called rotational transform — can be generated either by helix-like toroidally closed coils ('helical windings') or by poloidally closed ('modular') coils with lateral excursions [24]. Even with planar coils [25], a considerable rotational transform can be obtained. A winding law of modular stellarator coils is described in [26], which was used to compute classical $\ell = 2$ and $\ell = 3$ stellarator fields as well as configurations with helical magnetic axes. By varying the parameters of the winding law, the magnetic field can be optimized with respect to physics criteria such as rotational transform, shear, magnetic well, MHD equilibrium and stability properties and with respect to technical constraints such as curvature of current filaments, current density and optimum access to the plasma. Major limitations of this approach are that the functional space in which coil variations have to be considered is very large — a given confinement region can be realized with many coil systems — and that parameter variations of the coils easily cause a deterioration of the aspect ratio.

In a second approach, which was used for devising *Wendelstein VII-AS* [27], the properties of the confinement region are optimized by composing the field from sets of harmonic functions; for example, Dommaschk potentials [28]. Within this procedure a surface current producing the optimized field can easily be determined on a surface bounding a toroidal domain. Coils are then obtained by discretizing the surface currents. Again, a major disadvantage of this procedure is that variation of the amplitudes of the harmonic functions easily leads to an increase in aspect ratio.

A third approach tries to overcome the above-mentioned limitations and starts from the observation that the magnetic properties of a stellarator equilibrium are completely determined by the geometry of the plasma boundary. Variation of this boundary led to the Helias stellarator (see Sec. II). In a practical sense, specifying this boundary also guarantees that magnetic surfaces will exist inside the boundary. Further, it decouples the discussion of the magnetic properties of a stellarator configuration from its realization by coils and so necessitates a new method of determining coils. For this purpose the NESCOIL code was developed [29] to solve a Neumann problem at the plasma boundary in which a surface current is determined, such that the normal component of the field B produced by it is minimized at the plasma boundary. The input for the code consists of two toroidal surfaces, S_1, a magnetic surface at the plasma boundary, and S_2, an appropriately chosen surface outside of, and thus enclosing, S_1. Both surfaces are represented in Fourier series of two angular variables $0 \le u \le 1$ and $0 \le v \le 1$ in the poloidal and toroidal directions, respectively,

$$r = \sum_{m=0,n=-n_b}^{m_b,n_b} r_{m,n} \cos 2\pi(mu + nv) \quad , \quad z = \sum_{m=0,n=-n_b}^{m_b,n_b} z_{m,n} \sin 2\pi(mu + nv)$$

$$\varphi = \frac{2\pi}{M} v \,,$$

where M is the number of toroidal periods, (r, z, φ) are cylindrical co-ordinates and the usual stellarator symmetry $r(u,v) = r(-u,-v), z(u,v) = -z(-u,-v)$ is assumed. The code calculates a current distribution on S_2 such that the normal component of its field $\mathbf{B}$ on the surface S_1 is minimized. The surface current lines on S_2 are defined by $\phi(u,v) = constant$, where ϕ can be written as

$$\phi(u,v) = \sum_{m=0,n=-N}^{K,N} \phi_{m,n} \sin 2\pi\,(mu + nv) - \frac{I_p}{M} v - I_t u \,,$$

where I_p and I_t are the prescribed values for the net poloidal and toroidal surface currents, respectively. The magnetic field in the domain bounded by S_2 depends only on the net poloidal current I_p and is independent of the net toroidal current I_t. This is because a current distribution with zero net poloidal and finite net toroidal current which does not generate a field inside S_2 can be added to the solution. This property offers the possibility of producing the magnetic field either by poloidally-closed modular coils ($I_t = 0$) or by torsatron-like toroidally-closed coils (I_p/I_t rational). Which of these solutions is advantageous depends on the structure of the stellarator field to be realized; while it has been shown that toroidal Heliacs do not lend themselves to modular realization [30], it turns out that Helias stellarators are quite well suited for this approach.

The approximate solution of the boundary value problem yields a vacuum field which is regular in the whole domain bounded by the outer surface S_2. The outer current-carrying surface can be shaped in such a way that the resulting surface current distribution is not too complicated and can be discretized into a finite number of feasible coils. Fig. 8 shows a magnetic surface of a classical $l = 2$ stellarator with 5 field periods as well as a portion of the current lines determined by the NESCOIL code on a circular toroidal surface. Similarly, by using a torus with elliptic cross-section rotating with the flux surfaces, the planar coils of the first 'modular stellarator' [25] can be reproduced.

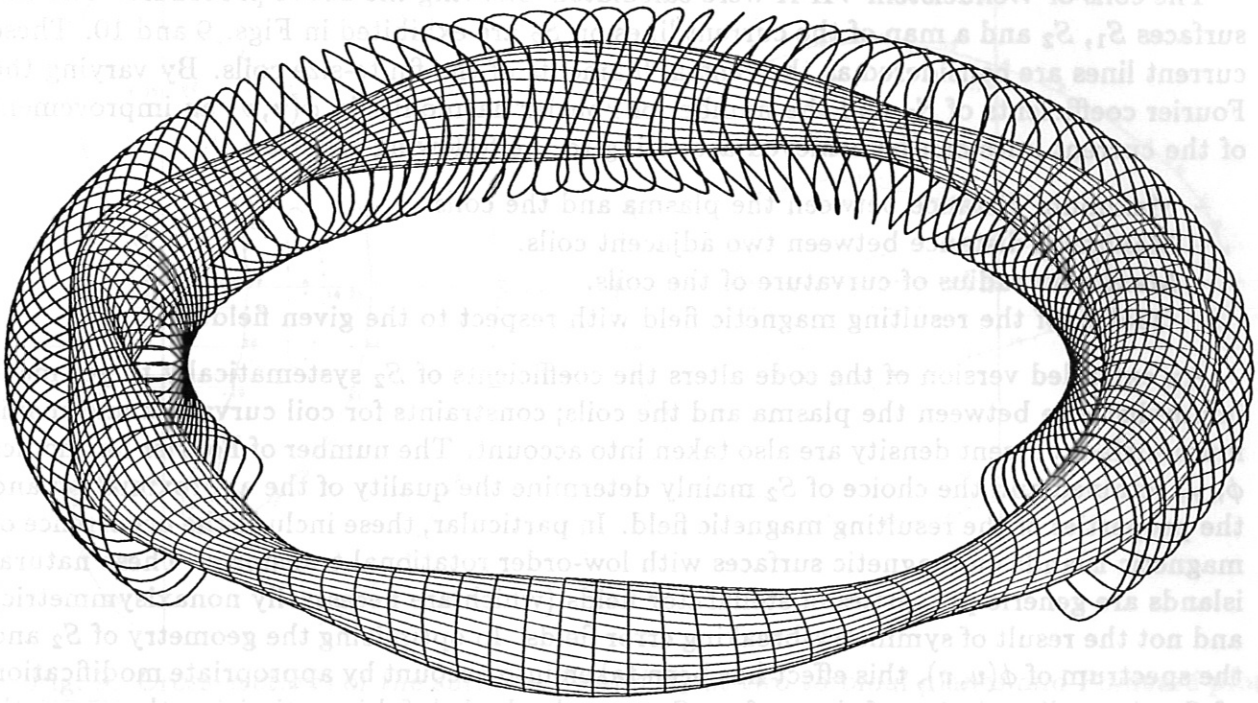

Fig. 8: *Magnetic surface of a classical $l = 2$ stellarator with 5 field periods and a portion of the current lines on a circular toroidal surface determined by the NESCOIL code.*

10.2 Optimization of the Coil System

The coils of *Wendelstein VII-X* were calculated following the above procedure. The two surfaces S_1, S_2 and a map of the current lines on S_2 are exhibited in Figs. 9 and 10. These current lines are considered as the central filaments of the finite-size coils. By varying the Fourier coefficients of S_2 and the number of Fourier harmonics in $\phi(u,v)$ an improvement of the current lines can be achieved according to the following criteria :

- Maximum distance between the plasma and the coils.
- Maximum distance between two adjacent coils.
- Maximum radius of curvature of the coils.
- Quality of the resulting magnetic field with respect to the given field.

An extended version of the code alters the coefficients of S_2 systematically to get maximum distance between the plasma and the coils; constraints for coil curvature and maximum surface current density are also taken into account. The number of Fourier harmonics $\phi_{n,m}$ retained and the choice of S_2 mainly determine the quality of the approximation and the properties of the resulting magnetic field. In particular, these include the occurrence of magnetic islands on magnetic surfaces with low-order rotational transform. These natural islands are generic properties of stellarator fields (which are necessarily nonaxisymmetric) and not the result of symmetry-breaking error fields. In optimizing the geometry of S_2 and the spectrum of $\phi(u,v)$, this effect has been taken into account by appropriate modification of S_2. A small variation of the surface S_1 may also be helpful in optimizing the magnetic field with respect to natural islands without adversely affecting the other properties of the magnetic field.

Locally the current lines calculated by NESCOIL may be too dense or too curved and therefore a local smoothing has been introduced. The deviation from the orginal field introduced by this smoothing has to be acceptable and limits this procedure. Such a coil set of one field period before and after smoothing is shown in the two parts of Fig. 11. The average major radius is $R_0 = 6.5$ m with the coils being arranged on a helix-like curve which has a maximum distance of 0.2 m from this axis. HS-5-8, for example, has the following geometric data: minimum radius of curvature 30 cm, minimum lateral distance between coil centers 22 cm and a minimum radial distance of 36 cm between the current surface (coil center) and a flux surface with an aspect ratio of 9.

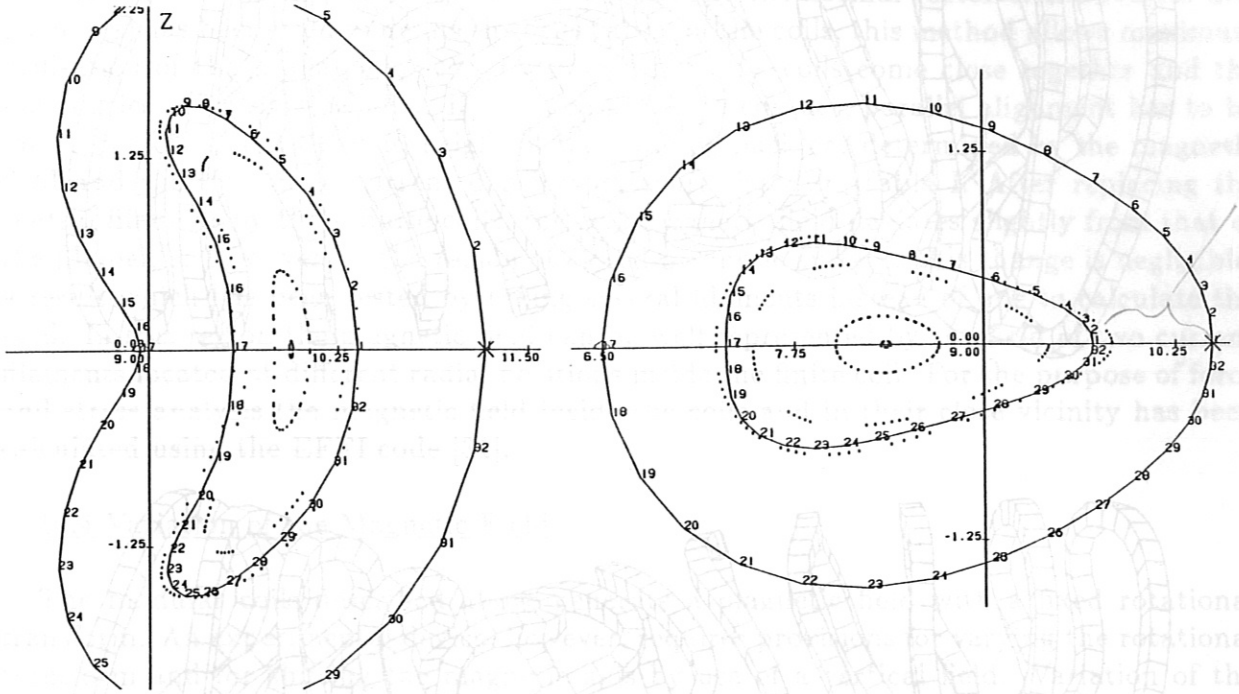

Fig. 9: *Cross-sections of the surfaces S_1 and S_2 at two toroidal planes and Poincaré plots of the magnetic field produced by the current filaments shown in Fig. 10.*

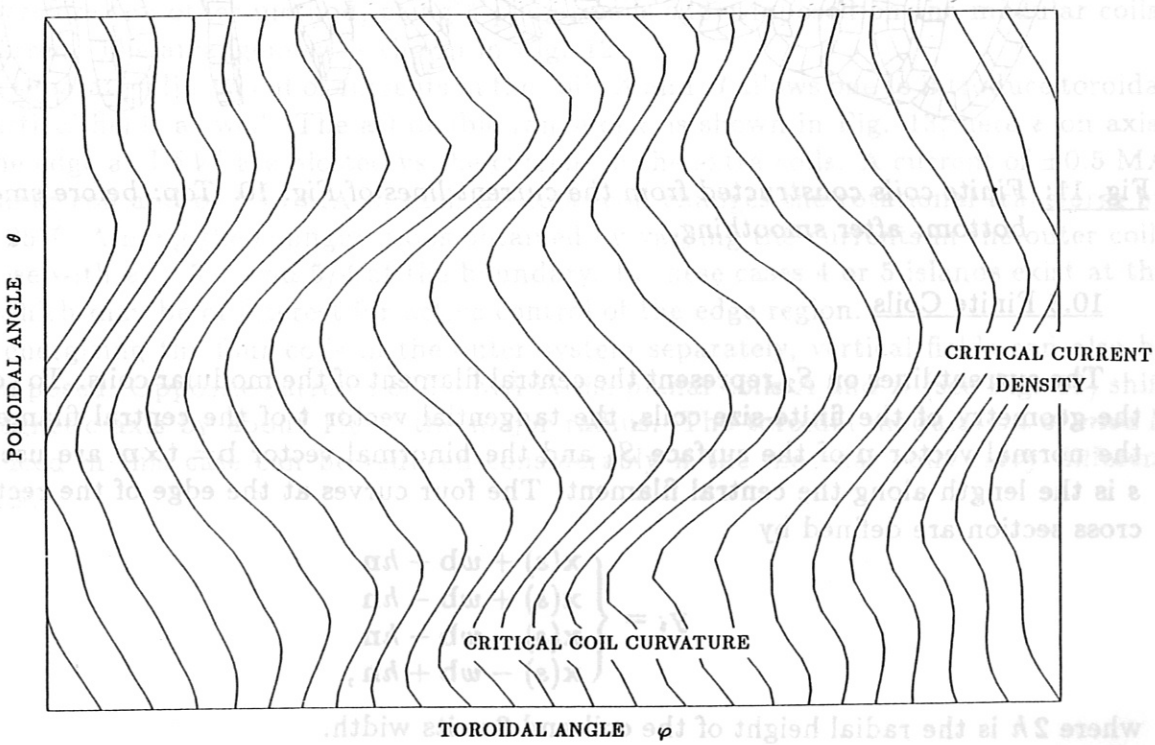

Fig. 10: *Surface current lines on S_2 for HS-5-8 as calculated by the NESCOIL code. One field period is shown.*

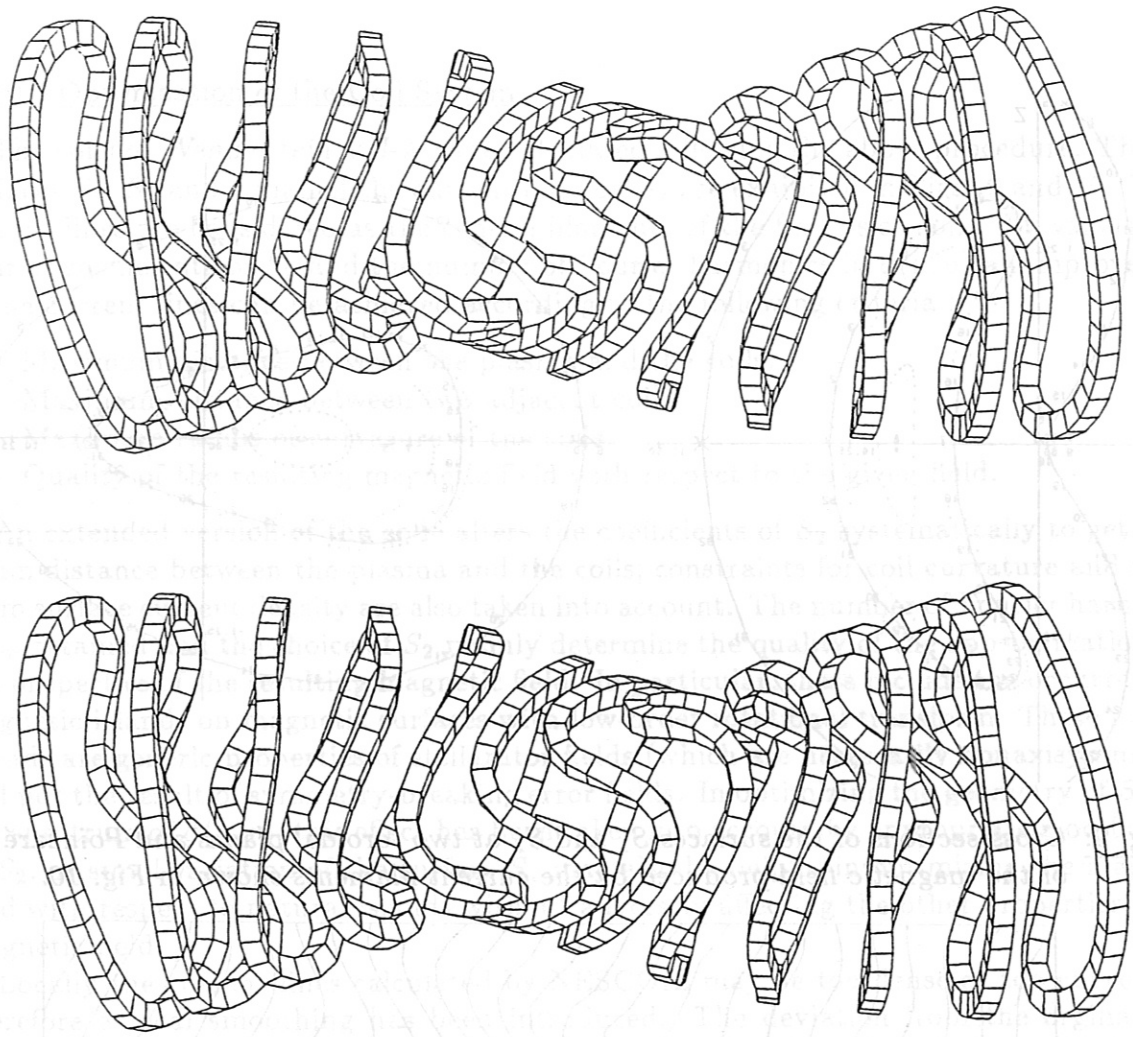

Fig. 11: *Finite coils constructed from the current lines of Fig. 10. Top: before smoothing, bottom: after smoothing.*

10.3 Finite Coils

The current lines on S_2 represent the central filament of the modular coils. To construct the geometry of the finite-size coils, the tangential vector $\mathbf{t}$ of the central filament $\mathbf{x}(s)$, the normal vector $\mathbf{n}$ of the surface S_2 and the binormal vector $\mathbf{b}= \mathbf{t}\times\mathbf{n}$ are used. Here s is the length along the central filament. The four curves at the edge of the rectangular cross section are defined by

$$\mathbf{y}_i = \begin{cases} \mathbf{x}(s) + w\mathbf{b} + h\mathbf{n} \\ \mathbf{x}(s) + w\mathbf{b} - h\mathbf{n} \\ \mathbf{x}(s) - w\mathbf{b} - h\mathbf{n} \\ \mathbf{x}(s) - w\mathbf{b} + h\mathbf{n}\,, \end{cases}$$

where $2h$ is the radial height of the coil and $2w$ its width.

Since the normal vector of the surface S_2 and not the normal vector of the central filament $\mathbf{x}(s)$ has been used to define the orientation of the coils, this method allows maximum utilisation of the available space, especially where the coils come close together and the boundaries are nearly parallel. If coils are nearly in contact, parallel alignment has to be made locally. The width and height of the winding pack are determined by the magnetic field and the maximum current density; data are listed in Table I. After replacing the central filament by these finite coils, the real magnetic field deviates slightly from that of the filaments. However, in the region of closed magnetic surfaces this change is negligible, a result which has been tested by taking several filaments instead of one to calculate the field. In this region the magnetic field can be well represented by the field of two current filaments located at different radial positions inside the finite coil. For the purpose of force and stress analysis the magnetic field inside the coils and in their close vicinity has been calculated using the EFFI code [31].

10.4 Variation of the Magnetic Field

The modular coils described above generate a magnetic field with a fixed rotational transform. An experimental device, however, requires provisions for varying the rotational transform and for shifting the magnetic axis by use of a vertical field. Variation of the rotational transform can be achieved by an additional set of external coils or by radially divided coils where the lower and upper layers can be energized separately [32]. This double layer concept, however, is rather inefficient in a large coil system with relatively slim coils and therefore the other method, using 4 planar coils superimposed on the modular coils, is preferred. The arrangement is shown in Fig. 12.

The separate adjustment of currents in the coils A and B allows one to introduce toroidal and vertical fields as well. The attainable range of ι is shown in Fig. 13; here ι on axis, ι at the edge and $\delta V'$ are plotted vs the current in the extra coils. A current of ± 0.5 MA per planar coil and of 1.75 MA in each modular coil changes the rotational transform by about 25%. Among the configurations obtained by varying the currents in the outer coils are those with $\iota = 5/5$ and $5/4$ at the boundary. In these cases 4 or 5 islands exist at the edge, which may be of interest for active control of the edge region.

By energizing the four coils in the outer system separately, vertical fields can also be superimposed. Opposite currents of 0.5 MA in the planar coils A and B (see Fig. 12) shift the magnetic axis by about 1% of the major radius. The toroidal modulation of $mod\, B$ introduced in this case can be reduced considerably if the modular coils carry different currents.

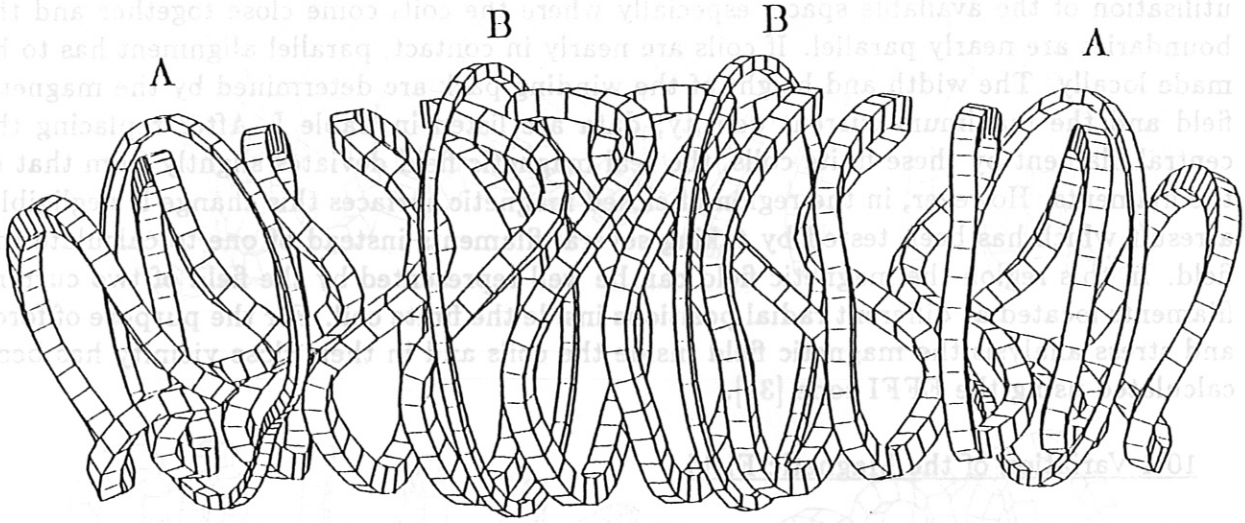

Fig. 12: *One field period of HS-5-8 showing modular coils and external planar coils A and B for varying the rotational transform and axis position.*

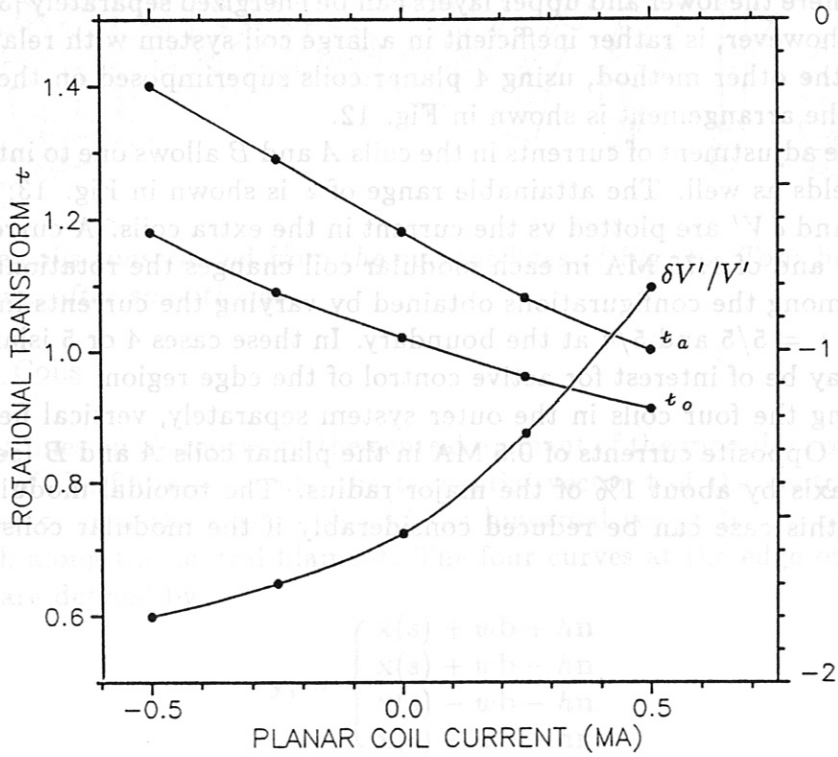

Fig. 13: *Configuration HS-5-8. Rotational transform ι_o on axis, ι_a at the edge, and the magnetic well $\delta V'/V'(0)$ as functions of the current in the planar coils. The current in the modular coils is 1.75 MA.*

10.5 Coil Design

The choice of superconducting coils for *Wendelstein VII-X* offers the possibility of steady-state operation, limited only by the capabilities of the heating schemes and the heat removal system. (At the maximum heating power of 20 MW a pulse duration of no more than 10 - 30 seconds appears possible; at reduced power, however, a truly steady-state experiment is possible.) The maximum field at the conductor is less then 6 T, allowing the use of NbTi as the superconducting material with a current density of 50 MA/m^2 averaged over the winding pack of the coils. The dimensions of the nearly rectangular coil cross section are 0.18 m $\times$ 0.2 m and the total current in each coil is 1.75 MA. Several options for superconducting cables have been investigated [33], leading to a 'cable-in-conduit' conductor as the optimum solution due to its high cryogenic stability. Cooling is provided by liquid helium and forced-flow cooling. The cross section of the superconducting cable is determined largely by the minimum radius of curvature — 30 cm for HS-5-8, limiting the cross section to 2 cm^2 with a maximum current of 10 kA. The details of the superconducting cable are being investigated; the final choice will depend on performance tests of various cables and on the results of a test coil.

The technique to be employed in the winding of the coils is another important issue presently under investigation. Similar to the procedure applied to *Wendelstein VII-AS*, the single cables must be bent in three dimensions and wound mechanically into a mold. Careful control of this process must be provided to minimize the 'spring-back' effect. The cables are insulated by glass fiber tapes and impregnated by epoxy resin after completion of the winding process. Unlike the normal-conducting coils of *Wendelstein VII-AS*, the coils of *Wendelstein VII-X* must be enclosed in a stainless steel casing to give them sufficient mechanical stiffness. Geometric tolerances of 10^{-3} are required to avoid field errors; the experience with manufacturing the modular coils of *Wendelstein VII-AS* has shown that a precision of this order is feasible.

Strong transient magnetic fields are not expected in the coil system and therefore eddy currents do not require enhanced cooling. Transient fields outside the plasma region do occur during the heating phase of the plasma; however, in the region of the superconducting coils, these time derivatives are not larger than $\dot{B} \approx 0.1\ \mathrm{T\,s^{-1}}$.

10.6 Normal-conducting Coils

Normal-conducting coils in *Wendelstein VII-X* would not present major technical difficulties since the same technique developed for *Wendelstein VII-AS* could be applied. For comparison with the superconducting option, normal-conducting versions have been designed which show the limitations and restrictions of this alternative. These limitations are consequences of the large ohmic power dissipated in the coils and the available electrical energy. The temperature rise in the coils limits the flattop time of the magnetic field.

In order to study the electrical power needed, the total dissipated energy, and the temperature rise inside the coils two versions of the configuration HS-5-7 are considered and compared to the 4-periodic configuration HS-4-8. In the first case the radial thickness of the coils is increased to 40 cm and the space of the plasma is not constricted. In the second case with 50 cm radial coil thickness the available plasma space is decreased and the distances between the coils are a minimum. The copper filling factor of the coils is considered to be $f_F = 0.66$. In the numerical calculations the increase of the coil resistance caused by heating is taken into account. A nonlinear system of differential equations for the coil current $i(t)$ and the heat factor $y(t) = 1 + \alpha \Delta\vartheta(t)$ with the initial conditions $i(0) = 0$, $y(0) = 1$ is solved numerically. The excitation of the coil system is divided into three phases: the loading phase, the flat-top phase, and the discharge phase. The duration of the flat-top phase is identical with the pulse time t_p.

Parameter studies have been made with the major radius being varied from $R_0 = 5$ m to $R_0 = 7$ m at constant coil aspect ratio $A_c = R_0/r_c = 5$. The main results with respect to the system parameters mentioned above are summarized in the following:

- In order to minimize the above values for a given magnetic field on axis the current density in the coils has to be as low as possible. This means maximization of the coil cross-sections and the copper volume of the coils.
- The HS-5-7 coil system is characterized by a current concentration at the positions $\varphi = i\,\frac{2\pi}{M}$, $i = 0, ..., M-1$, $M = 5$, at the coil sides facing the torus centre. Therefore the covering factor f_B is relatively low compared with 4-periodic coil configurations. This results in relatively high current densities in the coils and short pulse times. For 4-period coil configurations the current density in the coils is decreased. This offers the possibility to lower the values of energy consumption and to extend the pulse time.
- Assuming a maximum temperature rise in the coils of $\Delta\vartheta_{max} = 50$ K, the pulse time of the flat-top phase is between $t_p = 4.3$ s and $t_p = 7.5$ s in the systems considered.
- The lowest values of the maximum electrical power and the total dissipated energy attainable are $P_{max} \approx 780$ MVA and $W_{tot} \approx 5600$ MJ for the coil system HS-5-7 with $R_0 = 6.5$ m and coil cross-sections of 0.5×0.18 m. This dense package results in a total copper volume of $V_{Cu} = 32.4$ m^3. The pulse time of the flat-top phase is $t_p = 7.5$ s at a maximum temperature rise of $\Delta\vartheta_{max} = 50$ K.
- In any case the power supply system at IPP Garching has to be extended if a normal-conducting coil system for the W VII-X experiment is taken into consideration.

XI. Electromagnetic Forces

Magnetic forces on the modular coils are one of the main technical problems in *Wendelstein VII-X* . These forces determine the geometry of the support system and the mechanical stresses, thereby setting the technical limits of the coil system. The magnetic field inside the coils and the magnetic forces are calculated using the EFFI code [31]. A complex magnetic field distribution exists inside the coils, which leads to an inhomogeneous force distribution and a resulting net force on each coil pointing not only in the radial direction but also in the vertical and lateral directions as well. Fig. 14 shows the contour lines $mod\, B = constant$ in the $z = 0$ plane for two adjacent coils of HS-5-8; the maximum field at the coil boundary in this plane is 5.4 T. Forces and stresses have been calculated for a 4-period configuration HS-4-12 (major radius 5 m, $B_0 = 4$ T) and for HS-5-7 (major radius 6.5 m, $B_0 = 3$ T; see Table I). In order to describe the forces, the local orthogonal coordinate system defined by the vectors $\mathbf{n}$, $\mathbf{b}$, and $\mathbf{t}$ of section 10.3 is used. Hence, according to $\mathbf{f} = \mathbf{j} \times \mathbf{B}$, there are two components of the magnetic force density perpendicular to the direction of the current; f_R is the component in the direction of $\mathbf{n}$ (radial) and f_S the component in the direction of $\mathbf{b}$ (lateral). The component in the direction of $\mathbf{t}$ is zero ($f_T = 0$). Due to the 5-fold symmetry of the magnetic field and the symmetry within one field period, there are only 6 different coils, which facilitates the analysis appreciably. As an example, the average force density of two coils in HS-5-8 is shown in Fig. 15. The magnitude of the lateral force density may be comparable to the radial force density. This, in particular, occurs in those coils with strong lateral excursions and strong local curvature.

For the system HS-5-8 with $R_0 = 6.5$ m, the toroidal excursions of the coils are increased in comparison with the former system HS-4-12 with $R_0 = 5$ m. The result is an increase in the lateral force densities to levels where they can exceed the radial components; see Fig. 15. Although the magnetic field has been decreased from $B_0 = 4$ T to $B_0 = 3$ T in HS-5-8, the magnitude of the force densities is in the same range as for the coil system HS-4-12.

The moderate helicity of the magnetic axis of Helias coil systems causes a related helicity in the net coil force vector, corresponding to different coil forces in the radial and vertical directions. The resulting net forces are shown in Figs. 16 (HS-4-12) and 17 (HS-5-8). In the latter case, some coils even feel a force directed radially outward while others experience a force in the vertical direction which leads to a torque on the field period. The net force on the whole period is directed towards the torus center. As in the case of the local force densities, the maximum net forces are also comparable in HS-4-12 and HS-5-8. The maximum net force in both cases is 4 MN; under fault conditions — quenching of a coil — this force may increase to about 7 MN. It is of interest to compare these data with the centripetal forces of a system with equivalent circular planar coils; in such a case the net radial force per coil would be 2.3 MN.

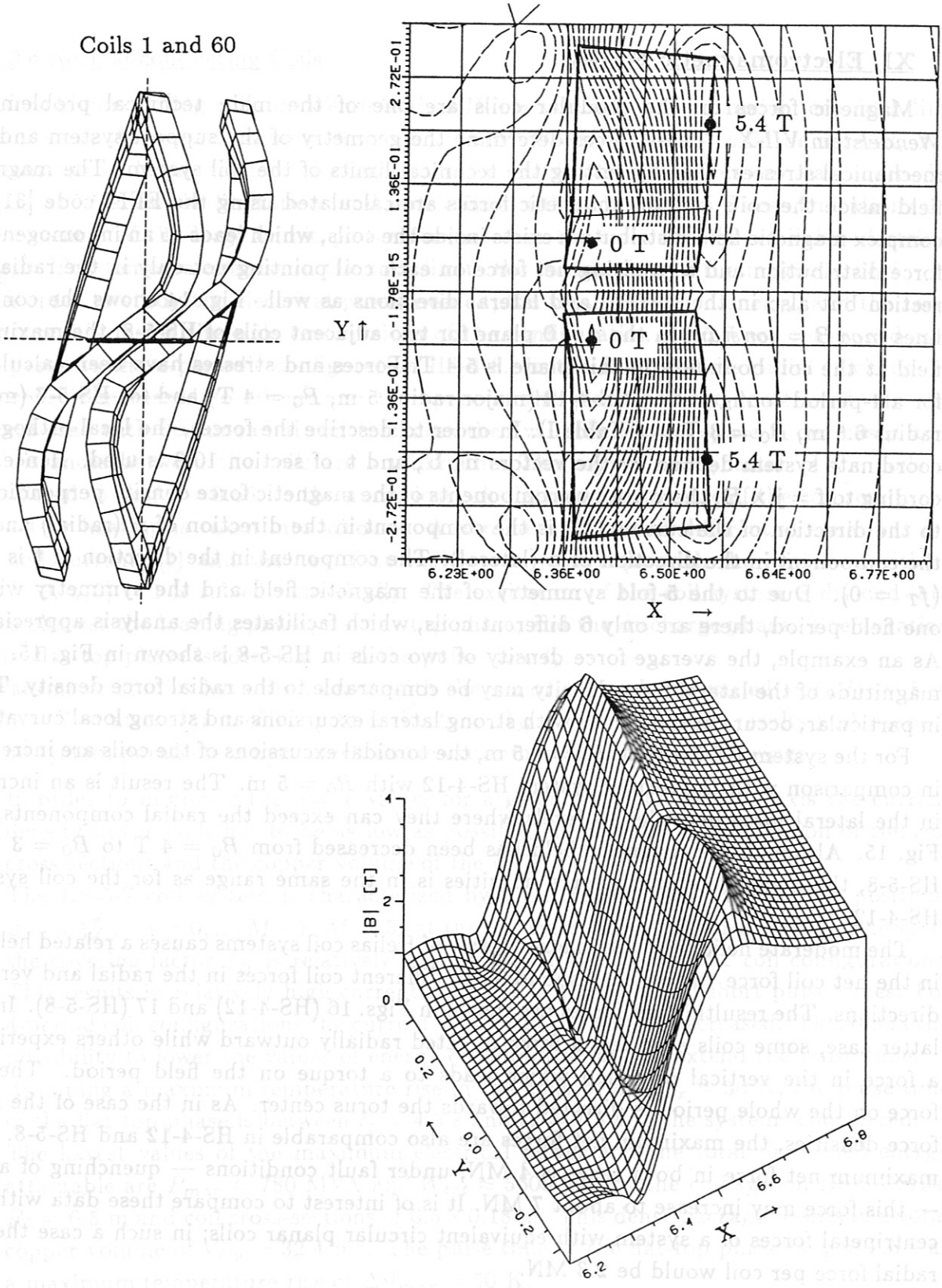

Fig. 14: *Contour lines B = constant in the $z = 0$ plane at coils 1 and 60 for HS-5-8. The maximum field is 5.4 T. The lower picture is a 3-D plot of B in the same plane.*

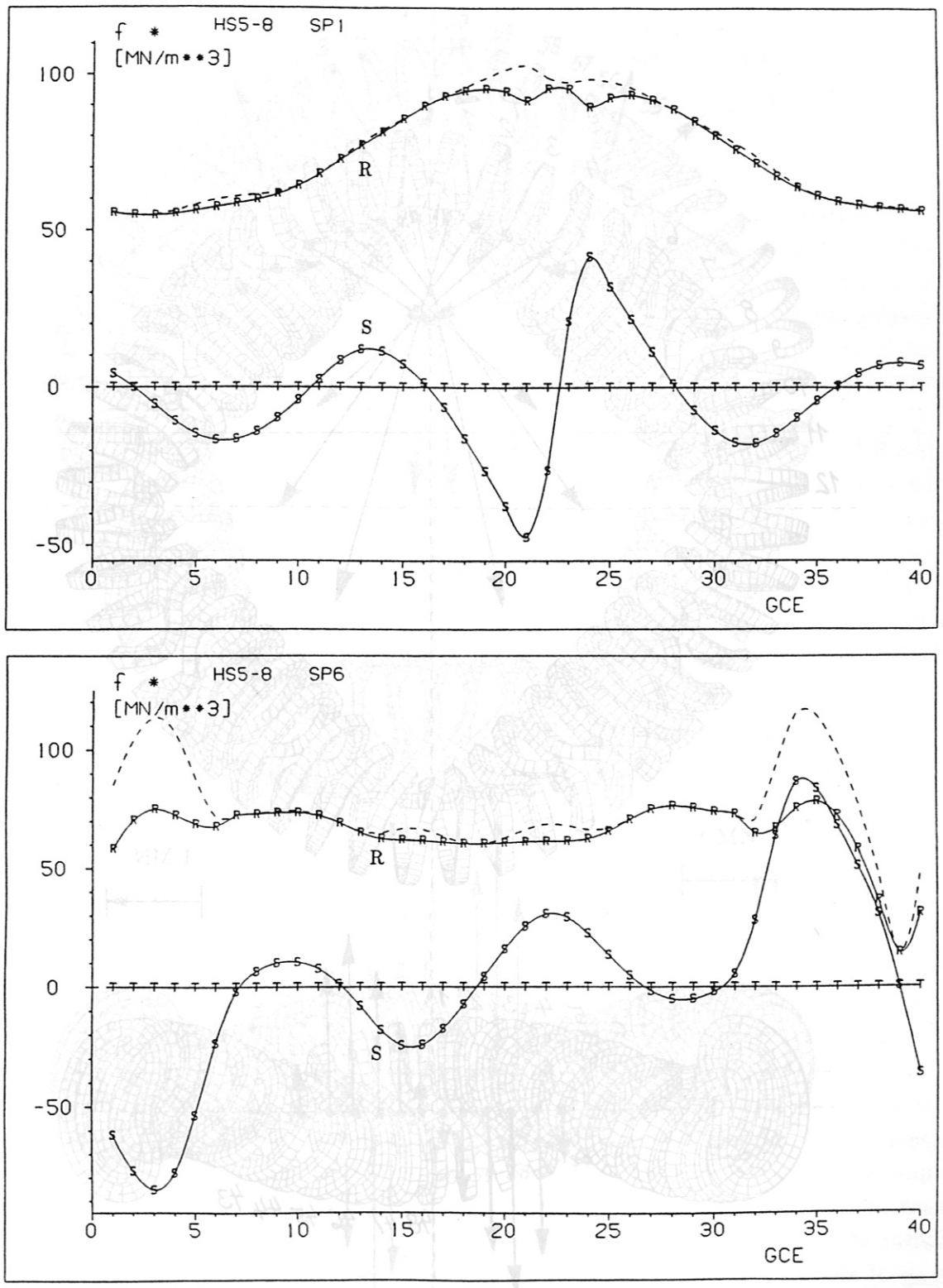

Fig. 15: *HS-5-8: Magnetic force densities in the radial (R) and lateral (S) directions for coils 1 (top) and 6 (bottom) as a function of the coil circumference (GCE=0 being the radial outside in the midplane of the coil). The dashed lines indicate the magnitude of the force density.*

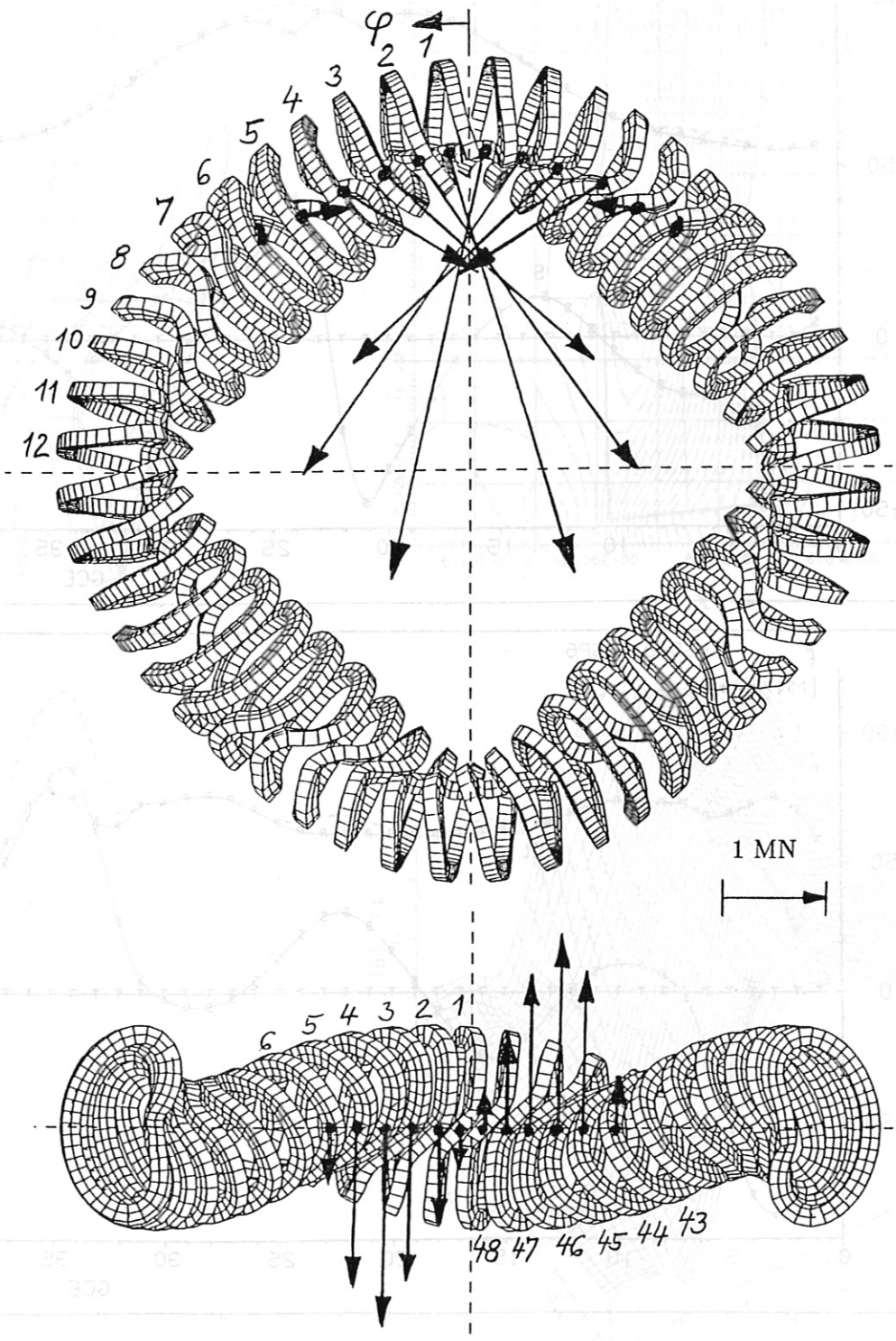

Fig. 16: *Coil system of HS-4-12 with net radial and vertical coil forces.*

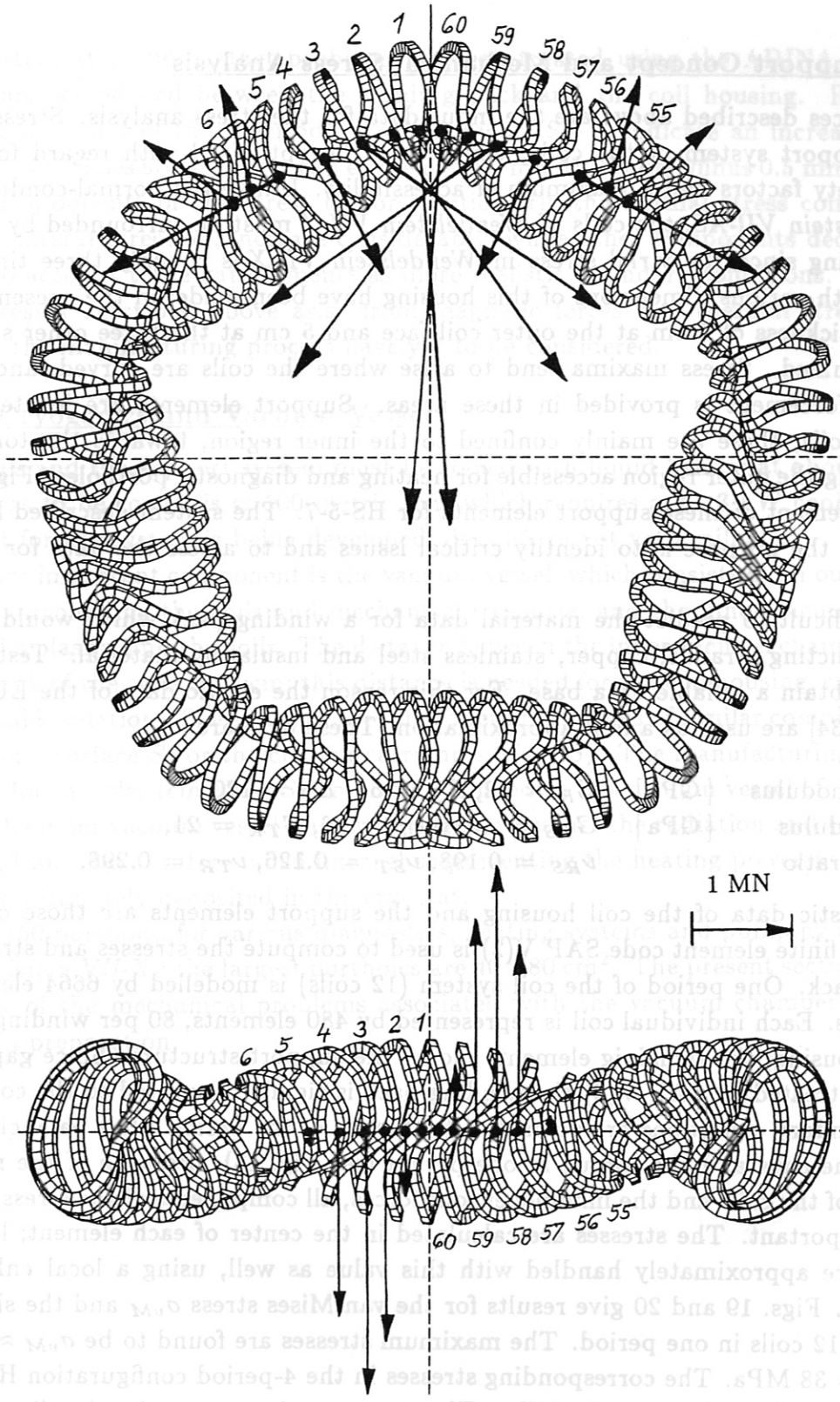

Fig. 17: *Coil system of HS-5-8 with net radial and vertical coil forces.*

XII. Support Concept and Mechanical Stress Analysis

The forces described above are the input data for the stress analysis. Stresses depend on the support system of the coils, which must be optimized with regard for material limits, safety factors and a maximum of accessibility. Unlike the normal-conducting coils of *Wendelstein VII-AS*, the coils of *Wendelstein VII-X* must be surrounded by a stainless steel housing since the virial stress in *Wendelstein VII-X* is roughly three times larger. Studies with various dimensions of this housing have been made; in the present results a housing thickness of 8 cm at the outer coil face and 5 cm at the three other sides of the coil is assumed. Stress maxima tend to arise where the coils are curved, and therefore extra reinforcement is provided in these areas. Support elements are located between adjacent coils; these are mainly confined to the inner region, towards the torus center, thus leaving the outer region accessible for heating and diagnostic portholes. Fig. 18 shows the arrangement of these support elements for HS-5-7. The system described here is not optimized; the purpose is to identify critical issues and to assess the data for a detailed design.

It is difficult to predict the material data for a winding pack which would consist of superconducting strands, copper, stainless steel and insulating material. Tests must be made to obtain a reliable data base. For this reason the elastic data of the EURATOM-LCT coil [34] are used as a first approximation. These data are:

Young's modulus	[GPa]	$E_R = 62, E_S = 53, E_T = 120,$
Shear modulus	[GPa]	$G_{RS} = 10, G_{ST} = 26, G_{TR} = 21,$
Poisson's ratio		$\nu_{RS} = 0.198, \nu_{ST} = 0.126, \nu_{TR} = 0.298.$

The elastic data of the coil housing and the support elements are those of stainless steel. The finite element code SAP V(2) is used to compute the stresses and strains in the winding pack. One period of the coil system (12 coils) is modelled by 6664 elements and 9600 nodes. Each individual coil is represented by 480 elements, 80 per winding pack and 400 per housing; the remainig elements model the support structure. Since gap elements cannot be treated by SAP V(2) the winding pack is rigidly connected to the coil housing. Fixed boundary conditions are defined at both ends of the period, thus balancing the net force on the coils and the torque in one period (see Fig. 18). Because of the non-planar geometry of the coils and the inhomogeneous forces, all components of the stress tensor are equally important. The stresses are calculated in the center of each element; local stress maxima are approximately handled with this value as well, using a local enhancement factor of 2. Figs. 19 and 20 give results for the van Mises stress σ_{vM} and the shear stress σ_{ST} of all 12 coils in one period. The maximum stresses are found to be $\sigma_{vM} \approx 140$ MPa and $\sigma_{ST} \approx 38$ MPa. The corresponding stresses in the 4-period configuration HS-4-12 are $\sigma_{vM} \approx 115$ MPa and $\sigma_{ST} \approx 32$ MPa. The stress maxima are rather localized and it is expected that these stresses can be reduced by optimizing the support system.

In a further step the contact problem has been treated using the ADINA code. Gap elements are introduced between the winding pack and the coil housing. First results obtained with coil 1 of the 4-periodic configuration HS4-11 indicate an increase of about 30% of the von Mises stress, using gap elements of 5 mm thickness minus 0.5 mm free space. Separate components of the stress tensor, particularly the normal stress components in radial and lateral direction, increase considerably; while other components decrease when taking into account these gap elements as more realistic boundary conditions.

The stresses described above arise from magnetic forces and thermal stresses; those caused by the manufacturing process have yet to be considered.

XIII. Cryogenics and Vacuum Vessel

The coils and the support system must be cooled with liquid helium at about 4 K. The overall mass to be cooled is $\approx$ 500 metric tons which requires a 2 - 3 kW cooling system. A cryostat for the system is being developed; details are not yet available.

A further important component is the vacuum vessel, which consists of an outer vacuum chamber, surrounding the coils and mechanical supports, and the inner vacuum chamber between the plasma and the coils. The distance between the inner vacuum chamber and the winding pack of the coils is 14 cm; this distance is needed for the coil housing, cooling pipes and thermal insulation. The shape of the inner vacuum vessel is of similar complexity to the last magnetic surface S_1 or the current carrying surface S_2. The manufacturing procedure developed for *Wendelstein VII-AS* can also be applied to the vacuum vessel of *Wendelstein VII-X* . The inner vacuum vessel must be protected against the radiation and thermal load from the plasma by a water-cooled liner, thus preventing the heating power to the plasma from being ultimately deposited in the cryostat.

About 150 portholes for various diagnostics, heating systems and pumping are planned for *Wendelstein VII-X* ; the largest portholes are 40×80 cm^2. The present section identifies only a few of the mechanical problems associated with the vacuum chamber; a detailed design is in preparation.

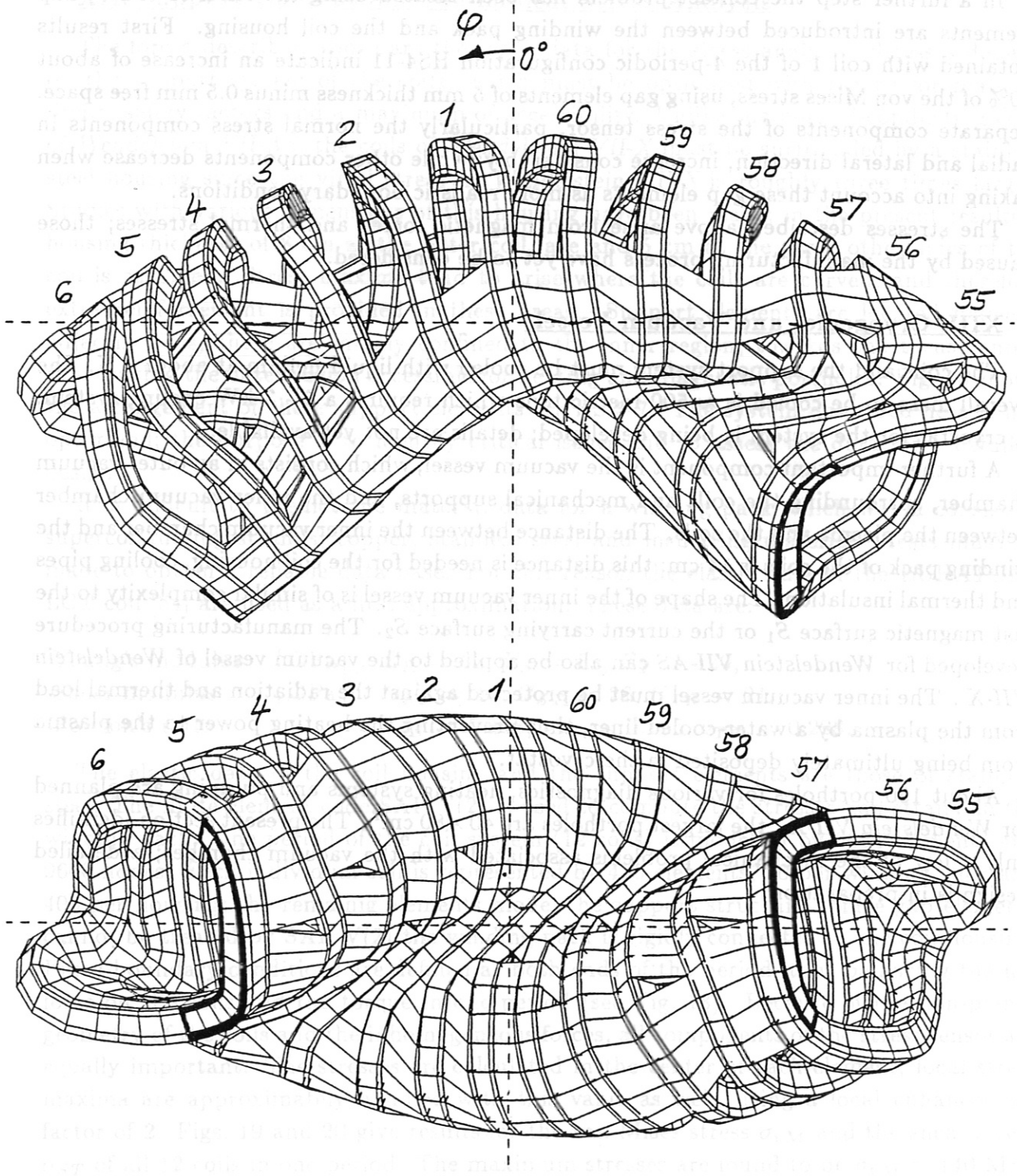

Fig. 18: *HS-5-7: Coils of one field period exhibiting the coil housing and the support elements. Fixed boundary conditions are placed on the solution at the positions indicated by heavier lineweight.*

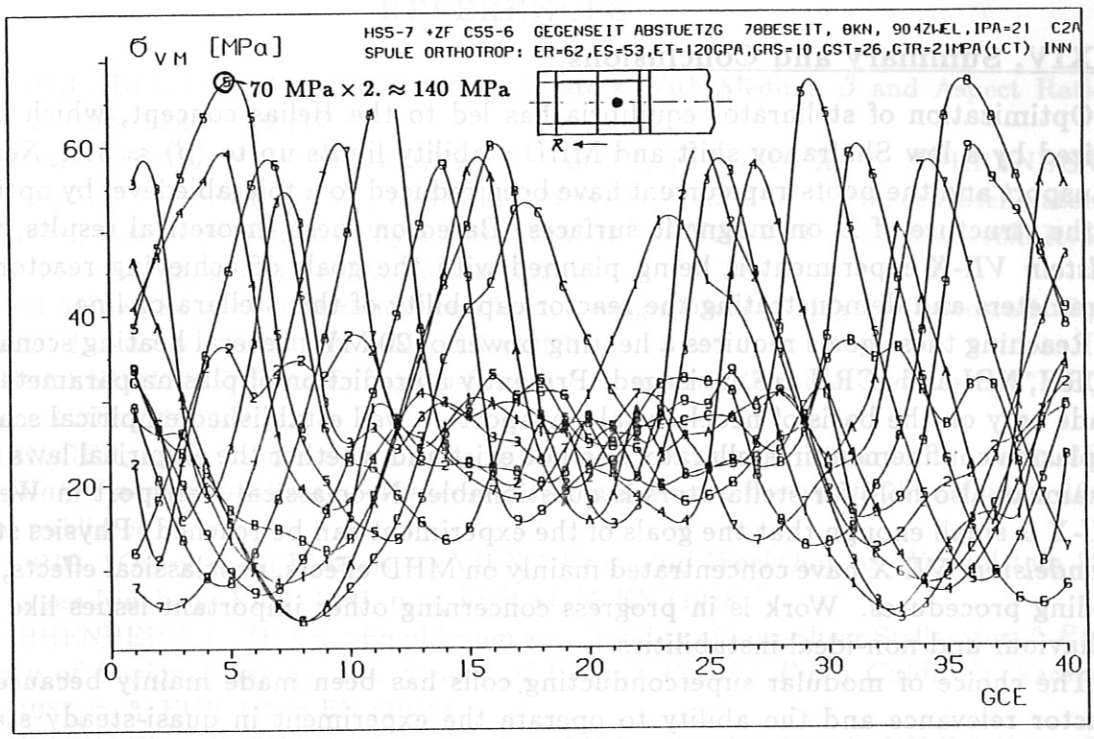

Fig. 19: *HS-5-7: Equivalent van Mises stress σ_{vM} along the coils of one field period. The labels on each curve refer to the 12 coils of one field period; for example, the curve labels 1-9,A,B,C correspond to the coils numbered 55 through 6 in Fig. 18. The insert indicates the stress output location.*

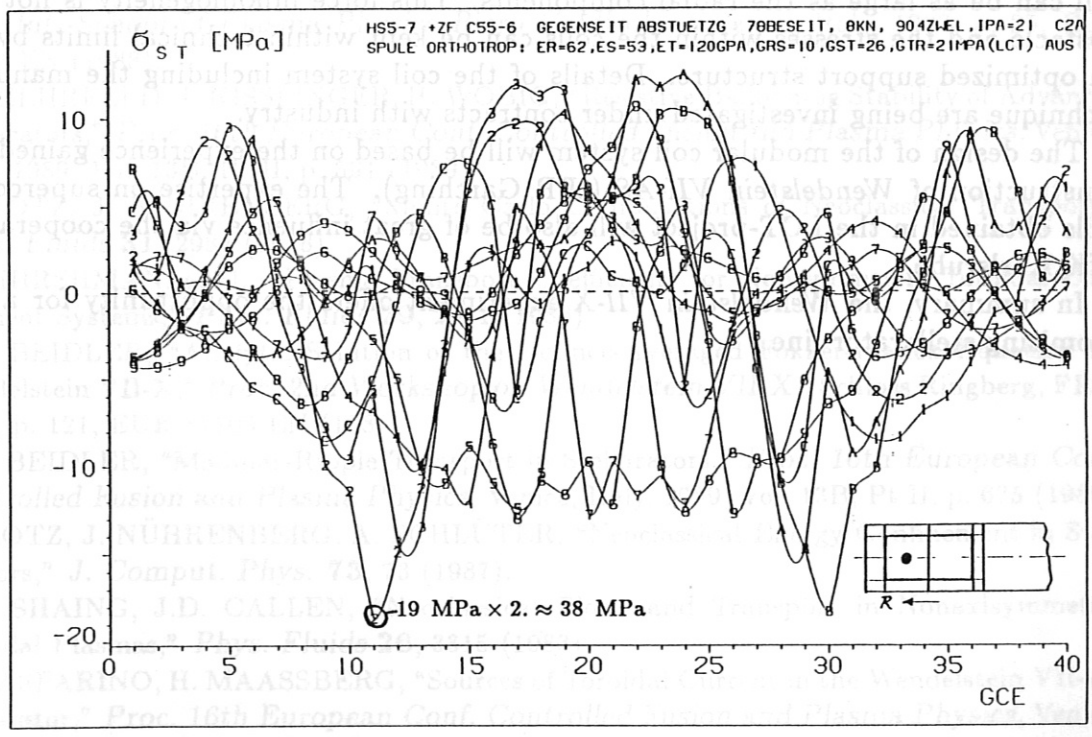

Fig. 20: *HS-5-7: Shear stress σ_{ST} along the coils of one field period. The curve labels are as given in Fig. 19.*

XIV. Summary and Conclusions

Optimization of stellarator equilibria has led to the Helias concept, which is characterized by a low Shafranov shift and MHD stability limits up to $\langle\beta\rangle \approx 5\%$. Neoclassical transport and the bootstrap current have been reduced to a tolerable level by optimization of the structure of B on magnetic surfaces. Based on these theoretical results, the *Wendelstein VII-X* experiment is being planned with the goals of achieving reactor-relevant parameters and demonstrating the reactor capability of this stellarator line.

Reaching these goals requires a heating power of 20 MW; several heating scenarios with ECRH, NBI and ICRH are envisaged. Presently a prediction of plasma parameters can be made only on the basis of neoclassical transport — well established empirical scaling laws of plasma confinement in stellarators do not exist and whether the empirical laws found for tokamaks also hold for stellarators is questionable. Neoclassical transport in *Wendelstein VII-X* is small enough that the goals of the experiment can be reached. Physics studies for *Wendelstein VII-X* have concentrated mainly on MHD effects, neoclassical effects, and coil-finding procedures. Work is in progress concerning other important issues like impurity behaviour and non-ideal instabilities.

The choice of modular superconducting coils has been made mainly because of their reactor relevance and the ability to operate the experiment in quasi-steady state. The superconducting coils of *Wendelstein VII-X* are the largest and most complex components of the experiment; for this reason, extensive studies have been made of the forces and stresses in this system. The net electromagnetic coil forces in modular Helias systems are inhomogeneous with components in all directions. Local lateral forces within a single coil can be as large as the radial components. This force inhomogeneity is not a serious obstacle and the stresses within the coils can be kept within technical limits by utilizing an optimized support structure. Details of the coil system including the manufacturing technique are being investigated under contracts with industry.

The design of the modular coil system will be based on the experience gained with the construction of *Wendelstein VII-AS* (IPP Garching). The expertise on superconducting coils obtained in the LCT-project will also be of great influence via the cooperation with KfK Karlsruhe.

In summary, the *Wendelstein VII-X* experiment offers the opportunity for a new and promising stellarator line .

REFERENCES

[1] J. NÜHRENBERG, R. ZILLE, "Stable Stellarators With Medium β and Aspect Ratio," *Phys. Letters* **114**A, 129 (1986).

[2] W. DOMMASCHK, F. HERRNEGGER, W. LOTZ, P. MERKEL, J. NÜHRENBERG, A. SCHLÜTER, U. SCHWENN, R. ZILLE, "Physics Studies for Advanced Stellarators," *Proc. 11th Int. Conf. Plasma Physics and Controlled Nuclear Fusion Research*, Kyoto, Japan, 1986, Vol. 2, p. 383, IAEA, Vienna (1987).

[3] D. PALUMBO, "Some Considerations on Closed Configurations of Magnetohydrostatic Equilibrium," *Il Nuovo Cimento* **X 53B**, 507 (1968).

[4] J. NÜHRENBERG, R. ZILLE, "Quasi-Helically Symmetric Toroidal Stellarators," *Phys. Letters* **129**A, 113 (1988).

[5] G. GRIEGER, et.al., "Physics Studies for Helical-Axis Advanced Stellarators," *Proc. 12th Int. Conf. Plasma Physics and Controlled Nuclear Fusion Research*, Nice, France, 1988, (to be published).

[6] H. WOBIG, "Overview on Wendelstein VII-X," *Proc. 2nd Workshop on Wendelstein VII-X* , Schloss Ringberg, FRG, 1988, p. 3, EUR 11705 EN (1988).

[7] J. NÜHRENBERG, R. ZILLE, "Equilibrium and Stability of Low-Shear Stellarators," *Proc. Theory of Fusion Plasmas, Int. School of Plasma Physics Piero Caldirola*, Varenna, Italy, 1987, p. 3, EUR 11336 EN (1988).

[8] J. NÜHRENBERG, R. ZILLE, "Optimization of Helias for Wendelstein VII-X," *Proc. 2nd Workshop on Wendelstein VII-X* , Schloss Ringberg, FRG, 1988, p. 17, EUR 11705 EN (1988).

[9] P. MERKEL, "Applications of the Neumann Problem to Stellarators: Magnetic Surfaces, Coils, Free Boundary Equilibrium, Magnetic Diagnostics," *Proc. Theory of Fusion Plasmas, Int. School of Plasma Physics Piero Caldirola*, Varenna, Italy, 1987, p. 25, EUR 11336 EN (1988).

[10] H.P. ZEHRFELD, J. KISSLINGER, H. WOBIG, "Resistive Ballooning Stability of Advanced Stellarators," *Proc. 16th European Conf. Controlled Fusion and Plasma Physics*, Venice, Italy, 1989, Vol. 13B, Pt II, p. 591 (1989).

[11] W. LOTZ, J. NÜHRENBERG, "Monte Carlo Computations of Neoclassical Transport," *Phys. Fluids* **31**, 2984 (1988).

[12] S.P. HIRSHMAN, et.al., "Plasma Transport Coefficients for Nonsymmetric Toroidal Confinement Systems," *Phys. Fluids* **29**, 2951 (1986).

[13] C.D. BEIDLER, "Analytic Solution of the Bounce-Averaged Fokker-Planck Equation for Wendelstein VII-X," *Proc. 2nd Workshop on Wendelstein VII-X* , Schloss Ringberg, FRG, 1988, p. 121, EUR 11705 EN (1988).

[14] C.D. BEIDLER, "Modular-Ripple Transport in Stellarators," *Proc. 16th European Conf. Controlled Fusion and Plasma Physics*, Venice, Italy, 1989, Vol. 13B, Pt II, p. 675 (1989).

[15] W. LOTZ, J. NÜHRENBERG, A. SCHLÜTER, "Neoclassical Energy Confinement in Stellarators," *J. Comput. Phys.* **73**, 73 (1987).

[16] K.C. SHAING, J.D. CALLEN, "Neoclassical Flows and Transport in Nonaxisymmetric Toroidal Plasmas," *Phys. Fluids* **26**, 3315 (1983).

[17] U. GASPARINO, H. MAASSBERG, "Sources of Toroidal Current in the Wendelstein VII-AS Stellarator," *Proc. 16th European Conf. Controlled Fusion and Plasma Physics*, Venice, Italy, 1989, Vol. 13B, Pt II, p. 631 (1989).

[18] C.D. BEIDLER, E. HARMEYER, F. HERRNEGGER, J. KISSLINGER, A. MONTVAI, F. RAU, R. SCARDOVELLI, H. WOBIG, "On the Edge Structure of a Helias Configuration," *Proc. 16th European Conf. Controlled Fusion and Plasma Physics*, Venice, Italy, 1989, Vol. 13B, Pt II, p. 699 (1989).

[19] D. HEIFETZ, D. POST, M. PETRAVIC, J. WEISHEIT, G. BATEMAN, "A Monte Carlo Model of Neutral-Particle Transport in Diverted Plasmas," *J. Comput. Phys.* **46**, 309 (1982).

[20] The LHS-Proposal (private communication).

[21] F.P. PENNINGSFELD, E. SPETH, "Neutral Injection into Wendelstein VII-X," *Proc. 2nd Workshop on Wendelstein VII-X* , Schloss Ringberg, FRG, 1988, p. 215, EUR 11705 EN (1988).

[22] U. GASPARINO, H. MAASSBERG, "Considerations on ECRH Current Drive and Bootstrap Current for Wendelstein VII-X," *Proc. 2nd Workshop on Wendelstein VII-X* , Schloss Ringberg, FRG, 1988, p. 157, EUR 11705 EN (1988).

[23] F. WESNER, "ICRH for Wendelstein VII-X," *Proc. 2nd Workshop on Wendelstein VII-X* , Schloss Ringberg, FRG, 1988, p. 221, EUR 11705 EN (1988).

[24] H. WOBIG, S. REHKER, "A Stellarator Coil System Without Helical Windings," *Proc. 7th Symp. Fus. Technology*, Grenoble, France, 1972, p. 345, EUR 4938 e (1972).

[25] S.N. POPOV, A.P. POPRYADUKHIN, "Production of a Helical Magnetic Field," *Soviet Physics - Technical Physics*, **Vol. 11, No. 2**, 284 (1966).

[26] E. HARMEYER, J. KISSLINGER, F. RAU, H. WOBIG, "A General Winding Law of Modular Stellarator Coils," Report IPP 2/274 (1985).

[27] U. BROSSMANN, W. DOMMASCHK, F. HERRNEGGER, G. GRIEGER, J. KISSLINGER, W. LOTZ, J. NÜHRENBERG, F. RAU, H. RENNER, H. RINGLER, J. SAPPER, A. SCHLÜTER, H. WOBIG, "Concept of an Advanced Stellarator," *Proc. 9th Int. Conf. Plasma Physics and Controlled Nuclear Fusion Research*, Baltimore, U.S.A., 1982, Vol. 3, p. 141, IAEA, Vienna (1983).

[28] W. DOMMASCHK, "Representations for Vacuum Potentials in Stellarators," *Comput. Phys. Comm.* **40**, 203 (1986); W. DOMMASCHK, "Solution to Stellarator Boundary Value Problems With a New Set of Simple Toroidal Harmonic Functions," *Z. Naturforsch.* **36a**, 251 (1981).

[29] P. MERKEL, "Solution of Stellarator Boundary Value Problems With External Currents," *Nuclear Fusion* **27**, 867 (1987).

[30] P. MERKEL, "Calculation of Coils for Stellarator Equilibria," *Proc. Workshop on Wendelstein VII-X* , Schloss Ringberg, FRG, 1987, p. 125, EUR 11058 EN (1987).

[31] S.J. SACKETT, "EFFI – A Code for Calculating the Electromagnetic Field, Force and Inductance in Coil Systems for Arbitrary Geometry," Lawrence Livermore National Laboratory Report UCRL-52402 (1978).

[32] J. KISSLINGER, E. HARMEYER, A. MONTVAI, F. RAU, H. WOBIG, "Magnetic Field, Force and Stress Calculations for Modular Helias Coil Systems," *Proc. 15th Symp. Fusion Technology*, Utrecht, The Netherlands, 1988, (to be published).

[33] W. MAURER, "General Aspects of Magnet Design for Wendelstein VII-X," *Proc. 2nd Workshop on Wendelstein VII-X* , Schloss Ringberg, FRG, 1988, p. 335, EUR 11705 EN (1988).

[34] A. MAURER, A. ULBRICHT, F. WÜCHNER, "Effect of Azimuthal Dependence of Radial Young's Modulus on the Mechanical Behavior of the European LCT Coil," *Proc. 9th Int. Conf. on Magnet Technology*, Zürich, Switzerland, 1985, p. 428 (1985).